Faculty of Mathematics and Physics
Charles University in Prague

FINAL YEAR THESIS

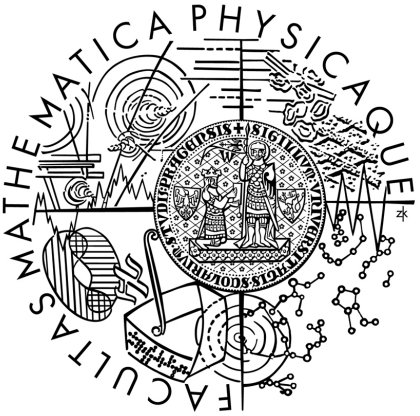

Interaction of line objects in ductile materials

Author: Josef Křišťan

Specialization: Mathematical and Computer Modeling in Science and Technology

Supervisor: Prof. RNDr. Jan Kratochvíl, DrSc.

Prague 11 August 2006

Chci zde vyjádřit veliké poděkování svému školiteli, Prof. RNDr. Janu Kratochvílovi, DrSc., za jeho cílené a obětavé odborné vedení. Neméně také vděčím svému kolegovi Ing. Vojtěchu Minárikovi za mnoho hodin strávených společnými diskusemi.

Tato práce je věnována mé mamince, Aleně Křišťanové, které chci tímto poděkovat za veškerou podporu během studia.

Prohlašuji, že jsem svou diplomovou práci vypracoval samostatně a výhradně s použitím citované literatury.

Souhlasím se zapůjčováním práce.

Josef Křišťan

Abstrakt

Dvě opačně orientované dislokace pohybující se po vzájemně rovnoběžných rovinách v tzv. PSB kanálu spolu interagují prostřednictvím svých elastických polí. Zpočátku uvažujeme dvě rovné konečné šroubové dislokace. Stěny kanálu jsou modelovány pomocí dislokačních dipólů. Dislokace nahrazujeme rovinnými křivkami. K numerickým simulacím byl vytvořen speciální počítačový program využívající metodu plovoucích objemů. Předpokládáme lineární vztah mezi velikostí rychlosti dislokace a silou, která na ni působí.

Během numerických simulací sledujeme změnu tvaru křivek při jejich pohybu a interakcích. Porovnáváme velikost napětí mezi křivkami při změně některých parametrů jako jsou vzdálenost skluzových rovin nebo šířka PSB kanálu. Analyzujeme dva případy, kdy kontrolujeme bud' vnější napětí nebo celkovou deformaci.

Klíčová slova: pohyb dislokací, metoda plovoucích objemů

Abstract

Two dislocations of opposite signs interacting via their elastic fields are consider. They move in parallel slip planes in a PSB channel. Initially they are kept apart in straight screw positions. The walls of the channel are simulated as the elastic field of rigid edge dipoles. The dislocations are modeled as plane curves. A special computer program based on the flowing volume method and the method of lines is employed. Assuming an over-damped motion, we consider a linear relationship between the force acting on the dislocation and the velocity magnitude.

The computation simulates the shape changes of the dislocations during their passing. The passing stress for various distances between the slip planes and for various channel width is compared with the bowing stress. The stress and strain controlled regimes of the dislocation motion are analyzed.

Keywords: dislocation dynamics, flowing volume method

Contents

Symbols

Symbol	Meaning
$\mathbf{b}; b$	Burgers vector; magnitude of Burgers vector
d_c	width of the PSB channel
E_{edge}	energy of edge dislocation
$\mathbf{F}_{\text{eff}}; F_{\text{eff}};$	effective force; its magnitude
$h; h_c$	distance between the slip planes; critical distance
$R(x)$	radius of curvature at a point x
$S(t)$	slipped area
t	time
T_{edge}	line tension of dislocation in edge orientation
T_{screw}	line tension of dislocation in screw orientation
v	velocity
$W; \delta W$	mechanical work; virtual work
α	angle between Burgers vector and a tangent to the disl. line
ε_{tot}	total shear strain
$\varepsilon_{\text{elas}}, p$	elastic and plastic part of total shear strain
Γ	dislocation curve
μ	shear modulus
ϱ	scalar density of the mobile dislocations
τ_{app}	applied shear stress
τ_{bow}	bowing stress
τ_{dip}	dipolar stress
τ, τ_{eff}	effective resolved shear stress in the slip plane
$\tau^{\star}_{\text{eff}}$	effective stress as a sum of bowing and dipolar stress
τ_{pass}	passing stress
$\tilde{\tau}$	stress tensor
ν	Poisson's ratio

Introduction

In a plastically deforming material, the obstacles to dislocation glide are usually more or less statistically distributed throughout the volume of the deformed material. On the other hand, there are interesting cases of plasticity in small volumes in which dislocation glide is confined locally, subject to some geometric constrain. Examples of current interest are the glide of dislocations in thin films. A related problem concerns the glide of dislocations in the channels between the di-/multipolar edge dislocation walls of the so-called ladder structure of persistent slip bands (PSBs) in fatigued metals. More generally, one is also interested in the constrained glide and interaction of the gliding dislocations. This is one of the cases that have been investigated recently by Pant, Schwarz and Baker [**1**] by dislocation dynamics simulations, as illustrated schematically in Fig. 1.

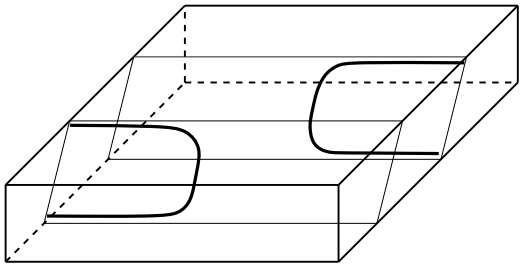

Figure 1: Interaction between threading dislocations on parallel glide planes.

In many of the early studies only the behaviour of a single dislocation segment was consider. Although the dynamics of an individual dislocation is a fairly well characterized phenomenon, the collective behavior of a large number of these defects appears to be an amazingly rich but poorly understood problem. For this reason the detailed understanding to the interaction between a pair of dislocations is attractive.

Pant et al. [**1**], using a dislocation dynamics approach, demonstrated that the configurations of the interacting dislocations of opposite sign can differ

significantly, depending on the relative magnitudes of the bowing and the dipolar interaction stress. The dislocations can either align to form a straight dipole (when the dipolar stress dominate) or pass each other in a curved configuration (when the bowing stress is much larger than the dipole passing stress). In the latter case, the strongly curved dislocations are not flexible enough to align as they do in the former case, when the dislocations are less strongly curved. As the dislocation segments bow out and advance, they draw out and deposit dislocations at the interfaces. In addition (confining ourselves to single slip), the dislocations must at the same time overcome the elastic interaction with dislocations of opposite sign which they encounter. Thus, two processes, namely Orowan bowing and dislocation dipole interaction are expected to make contributions to the flow stress.

In persistent slip bands formed by subjecting a ductile material to cyclic plastic strain, dislocations shuttle backwards and forwards between walls of densely-packed edge dislocation dipoles. The maximum stress achieved in any one hysteresis loop saturates after several hundred cycles, becoming constant with further cycling and defining the endurance limit in conventional fatigue tests. There are several possible contributions to the endurance limit (Brown [**2**]):
(i) the stress required to make screw dislocations of opposite sign pass one another, which is the same as the stress required to split apart screw dislocation dipoles between the walls; (ii) the stress required to bow the screw dislocations between the walls; (iii) internal stress resulting from inhomogeneous plastic deformation, caused by the resistance to plastic flow of the walls being much greater than dislocation-free material; (iv) friction stress which might come from dislocation debris left between the walls by the shuttling screw dislocations.

The general model describing the behaviour of the dislocations in the channel is formulate in Chapter 1. In Chapter 2 we mention the main relations for dislocation curves. The proposed structure of the walls of the PSB channel will be discuss in Chapter 3. Basic dynamics properties of dislocations and analysis of stress distribution in the slip planes is given in Chapter 4. The mathematical description of an individual dislocation line is in Chapter 5 and system of equations describing the motion of dislocations including initial and boundary conditions is formulate in Chapter 6. We explain numerical scheme for computer simulations in Chapter 7. In Chapter 8 we discuss in more details numerical simulations. Finally, the results of the numerical simulations are in the concluding Chapter 9.

Chapter 1

Physical Background

Plastic deformation of crystalline solids is a result of the motion of dislocations. A dislocation is a line defect of the crystal lattice. Along the dislocation line the regular crystallographic arrangement of atoms is disturbed.

The dislocation line is represented by a closed curve or a curve ending at the surface of the crystal. At low homologous temperature the dislocations can move only along crystallographic planes with the highest density of atoms. The motion results in mutual slipping of the neighboring parts of the crystal along the slip planes. The slip displacement carried by a single dislocation, called Burgers vector, is equal to one of the vectors connecting the neighboring atoms.

The displacement field of atoms from their regular crystallographic positions around a dislocation line can be treated (except the close vicinity of the line) as the elastic stress and strain field. On the other hand, a stress field exerts a force on a dislocation. The combination of these two effects causes the elastic interaction among dislocations.

One of the most distinguished features of plastic deformation at the microscale is a great overproduction of dislocations during a deformation process. Only a small friction of generated dislocations is needed to carry plastic deformation. The rest of them is stored in the crystal. The glide dislocations are moved by the shear stress resolved in the slip plane. The segments such dislocations extend over distances of micrometers and during deformation they become curved. The local curvature of the dislocations seems to be one of the leading factors of their motion.

The goal of the present work is to utilize the dislocation dynamics approach to gain a deeper understanding of some of the mechanisms of plastic deformation.

1.1 Models

First, we describe and analyse the two models proposed by Brown [**2, 3**] and Mughrabi & Pschenitzka [**4**] and their main results. Thereafter we will briefly describe our proposed model.

In paper [**3**] Brown considered only two contributions to the endurance limit. The stress required to make screw dislocations of opposite sign pass one another and the stress required to bow the screw dislocations between the walls. Mughrabi and Pschenitzka [**4**] have queried the latter assumption, and in a new calculation taking into account all four of the contributions listed above are able to reach agreement with the data for the saturation stress of copper at room temperature. In response to a recent paper by Mughrabi and Pschenitzka [**4**], in paper [**2**] Brown proposed and improved analytical formula which enable a quantitative account to be given of the saturation stress.

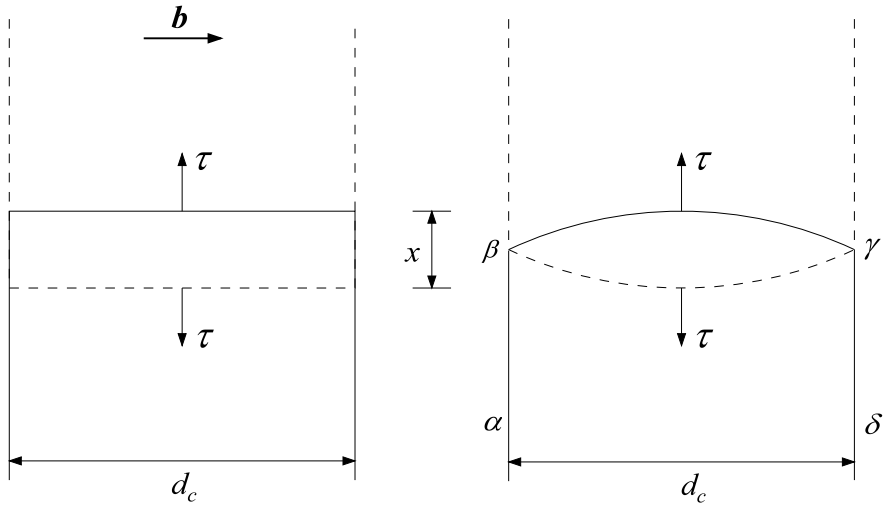

Figure 1.1: Brown (on the left hand side) and Mughrabi & Pschenitzka.

Brown 1

Figure 1.1, on the left hand side, shows the configuration analysed by Brown in [**3**]. Rigid screw dislocations of opposite sign must escape from one another while at the same time they deposit edge dislocations in the walls, between

which they are confined. The total separation stress required is simply

$$\tau = \frac{2E_{\text{edge}}}{bd_c} + \frac{\mu b}{4\pi h} \ . \tag{1.1}$$

The first term gives the contribution from bowing an isolated screw dislocation of Burgers vector $\mathbf{b}$ between walls of spacing d_c. The second term correspond to split an infinitely long screw dislocation dipole of height h. μ is the shear modulus and b the magnitude of the Burgers vector. E_{edge} denote the energy of edge dislocation per unit length. This can be thought as the screw dislocations pass one another on parallel planes of spacing h simultaneously with the bowing. The minimum value of h, say h_c, is the smallest spacing of stable screw dislocation dipole. For $h < h_c$ the screw dislocations annihilate one another by cross-slip. Hence, this critical value h_c corresponds to the largest possible dipole interaction, and determines the endurance limit.

Equation (1.1) can be derived by using principle of virtual work. Imagine the rigid screw dislocation to move forward by a virtual displacement δx. The work δW done by the total stress τ is $\delta W = F\delta x = \tau b d_c \delta x$. Here b is the magnitude of the Burgers vector, d_c walls spacing and F the force acting on the dislocation of the length d_c. This work includes depositing edge dislocations of energy per unit length E_{edge}, that is $2E_{\text{edge}}\delta x$, as well as currently overcoming the maximum spliting force of straight screw dipole, hence $\tau_{\text{pass}}^{\max} b d_c \delta x = (\mu b/4\pi h) b d_c \delta x$. Overall we have

$$2E_{\text{edge}}\delta x + \frac{\mu b}{4\pi h} b d_c \delta x = \tau b d_c \delta x \ . \tag{1.2}$$

Note that the energy of edge dislocation is given by relation:

$$E_{\text{edge}} = \frac{\mu b^2 \ln(d_c/r_0)}{4\pi(1-\nu)} \ , \tag{1.3}$$

Note, that in evolution of E_{edge} is d_c the width of the channel and r_0 the core radius is taken to be the Burgers vector length. ν is Poisson's ration.

Mughrabi and Pschenitzka

The approximation of rigid dislocations has been criticized by Mughrabi and Pschenitzka [**4**]. Since the relative magnitudes of the interacting stresses vary, depending on the momentary location of the dislocation, the total stress required will depend on the sum of the spatially varying bowing and the dipolar interaction stress contributions $\tau_{\mathrm{bow}}(x)$ and $\tau_{\mathrm{dip}}(x)$. Parameter x denotes the spacing between the two dislocations measured in the middle of the constrained glide plane. We obtain the dependence of the overall stress τ on x:

$$\tau(x) = \tau_{\mathrm{bow}}(x) + \tau_{\mathrm{dip}}(x) \ . \tag{1.4}$$

For the sake of simplicity, it is assumed that the overall stress situation can be reduced to a one-dimensional problem and can be approximated satisfactorily by considering only the interaction between the leading curved line elements of the two encountering dislocation segments in the centre of the channel.

As shown experimentally [**5**], the bowed-out screw dislocation can be considered to have an elliptical shape. It means that the curved segment extending across the channel of width d_c from one dislocation wall to the next is a part of an ellipse (major axis a_{e}, minor axis b_{e}, axial ratio of major to minor axis is $\kappa_{\mathrm{e}} = a_{\mathrm{e}}/b_{\mathrm{e}}$) as indicated in Fig. 1.2.

A truncated elliptical arc of dislocation is pushed by the applied stress between the walls. Simultaneously its partner of opposite sign is pushed in the opposite direction. The two dislocations attract one another and if their curvature is not great can be thought of as forming a dipole of width x and of height h determined by the spacing between their two slip planes. Eq. (1.4) will subsequently be evaluated quantitatively in detail:

$$\tau(x) = \frac{T_{\mathrm{screw}}}{bR(x)} + \frac{\mu b}{4\pi}\frac{2x}{x^2+h^2} \ . \tag{1.5}$$

First term, representing the stress contribution τ_{bow}, is written in terms of the dislocation line tension T_{screw} and the space-dependent radius of curvature $R(x)$ of the dislocation. The second term is simply the space-dependent dipolar shear stress τ_{dip} acting on a screw dislocation in the stress field of another screw dislocation of opposite sign, separated by a distance x and lying on a glide plane at a spacing h.

Let us derive the relation for the radius of curvature in the middle of the channel in terms of distance x and the channel width d_c, see Fig. 1.2. The point O is a centre of the local coordinate system xz. The condition that

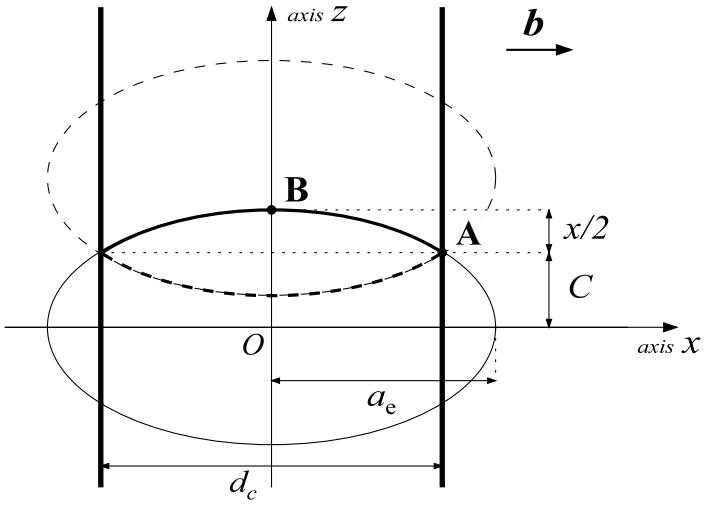

Figure 1.2: Model proposed by Mughrabi and Pschenitzka.

point A lies on the ellipse gives

$$\frac{\left(\frac{d_c}{2}\right)^2}{a_e^2} + \frac{C^2}{b_e^2} = 1 \ . \tag{1.6}$$

Multiplying Eq. (1.6) through by b_e^2 and using the fact that $b_e = C + x/2$ we can express

$$C = \frac{d_c - \kappa_e^2 x^2}{4\kappa_e^2 x} \ . \tag{1.7}$$

The critical Orowan configuration is given by $C = 0$ for $x = 2a_e/\kappa_e = d_c/\kappa_e$. The radius of curvature at the point B of the ellipse is

$$\begin{aligned} R(x) &= \frac{a_e^2}{b_e} = \left(\frac{a_e}{b_e}\right)^2 b_e = \kappa_e^2 b_e = \\ &= \kappa_e^2 \left(C + \frac{1}{2}x\right) = \frac{d_c^2 + \kappa_e^2 x^2}{4x} \end{aligned} \tag{1.8}$$

and Eq. (1.5) can be written for the stress to maintain the separation x in the form

$$\tau(x) = \frac{2T_{\text{screw}}}{b} \frac{2x}{d_c^2 + \kappa_e^2 x^2} + \frac{\mu b}{4\pi} \frac{2x}{x^2 + h^2} \ . \tag{1.9}$$

As the stress is increased from zero, the elliptical segments become more and more curved, until they become tangent to the wall, whereupon they escape

one another. This Orowan configuration correspond to $C = 0$ and determine the critical stress for flow.

Eq. (1.9) shows that as the separation between the screw dislocations increases, the stress required to maintain them in position goes through two maxima. One due to the bowing,

$$\frac{2T_{\text{screw}}}{b}\frac{2x}{d_c^2 + \kappa_{\text{e}}^2 x^2} \leq \frac{2T_{\text{screw}}}{b}\frac{1}{\kappa_{\text{e}} d_c} \ , \tag{1.10}$$

with equality at $x = d_c/\kappa_{\text{e}}$ and the other due to the passing,

$$\frac{\mu b}{4\pi}\frac{2x}{x^2 + h^2} \leq \frac{\mu b}{4\pi}\frac{1}{h} \ , \tag{1.11}$$

with equality at $x = h$. These two inequalities follows from $u^2 + v^2 \geq 2uv$ which hold for all $u, v \in \mathbb{R}^+$. The maximum passing stress occurs when the two screw dislocations are close enough to annihilate one another by cross-slip, which again defines a critical minimum dipole height h_c.

Mughrabi and Pschenitzka [**4**] plot the stress as a function of separation x. A general conclusion of their study is that the resulting stress is never a simple linear sum of the Orowan bowing stress and the dipole passing stress. Rather, the flow stress is always governed by the stronger of the two interactions. In the case of constrained dislocation glide in the channel of the PSB wall structure in fatigued metals, the dipole passing stress and the Orowan stress are of similar magnitude, and the local flow stress in the channel is found to be only about 20% larger than the stress due to either bowing or passing acting alone.

The calculation above leading to Eq. (1.9) is a considerable improvement upon the rigid dislocation approximation leading to Eq. (1.1). However, despite allowing the passing dislocations to be curved, it allows them only one 'degree of freedom' - namely the separation x. The separation determines both the bowing term and the dipole interaction.

Brown 2

In detailed description of the process of passing curves, in paper [**2**] Brown argued that the effect of trailing edge dislocations $\alpha\beta$ and $\gamma\delta$, see Fig. 1.1, is not taken into account. If we think only about bowing stress, which if it were to act alone, it has a maximum value equal to the Orowan stress and depend upon the energy of dislocations $\alpha\beta$ and $\gamma\delta$. These dislocations pull the elliptical sections towards one another. For this reason Brown think about a configuration with three degrees of freedom: the separation x as above, but now allowed to depend upon position x' in the channel, together with independently determined values of the radii of curvature of the dislocations near the walls and in the centre of the channel.

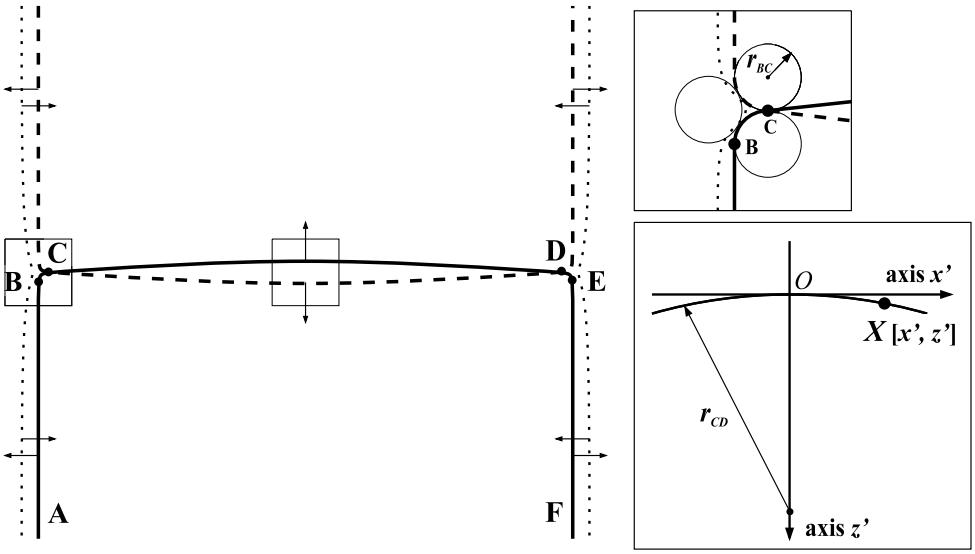

Figure 1.3: Improved model by Brown.

To get detailed picture about the shape of dislocation, let us consider three regions under the action of the applied stress, Fig. 1.3:
(i) Edge dislocations AB and EF experience zero force because their closely-spaced neighbour suffers an equal and opposite force, and the two dislocations comprising the dipole find an equilibrium configuration. Dislocations AB and EF are straight.
(ii) BC and DE - the crossing dislocations pull the edge dipoles apart and feel not only the applied stress, but also attraction for each other. Brown modelled this region by three touching circles. One expects the radii of curvature r_{BC} and r_{DE} to be very small.

(iii) Part CD: because the dislocations are on the point of passing one another, they feel the applied stress pushing them forward and the passing stress near its maximum pulling them back. This assumption can be done in case if we consider CD is a stiff screw dislocation with large radius of curvature. As a result of the curvature, not all the length CD experiences the maximum passing stress, but some average $\langle \tau_{\text{pass}} \rangle$.

We assume, that the instability arises from a small displacement δx. The principle of virtual work gives

$$2E_{\text{edge}}\delta x + \langle \tau_{\text{pass}} \rangle \, b(d_c - 2r_{BC})\delta x = \tau b d_c \delta x \ . \tag{1.12}$$

The goal is to estimate the average of passing stress $\langle \tau_{\text{pass}} \rangle$ and radius of curvature r_{BC}. From symmetry we have $r_{DE} = r_{BC}$. Brown considers, that radius r_{BC} is very small, less than a few percent of the channel width. In the situation without other dislocation, the force maintaining the curvature is $\tau b = T/r_{BC}$, where the appropriate line tension T might be for a mixed screw-edge dislocation. Following Fig. 1.3, let us imagine that the dislocations in the node-like triple-circle construction are distant on average from one another by the diameter of the inscribed circle, it is about $r_{BC}/3$. The approximate equation for equilibrium including the dislocation interactions is now

$$\left(T_{\text{mixed}} - \frac{3\mu b^2}{2\pi(1-\nu)} \right) = \tau b = \frac{T_{\text{eff}}}{r_{BC}} \ . \tag{1.13}$$

Now, we describe how to find the average passing stress, the dipole splitting stress, felt by the curved screw segments. The interaction stress between the two gently curved segments experiences the maximum at the centre of the channel. We expand the passing stress near its maximum as a function of the distance z' measured from where the screw would be if it were straight, see Fig. 1.3:

$$\tau_{\text{pass}}(z') = \frac{\mu b}{4\pi} \frac{2x}{x^2 + h^2}\bigg|_{x=h+z'} = \frac{\mu b}{4\pi} \frac{2z' + 2h}{z'^2 + 2hz' + 2h^2} \ . \tag{1.14}$$

The Taylor series that approximates the function $\tau_{\text{pass}}(z')$ around 0 is

$$\tau_{\text{pass}}(z') = \frac{\mu b}{4\pi} \left(\tilde{\tau}_{\text{pass}}(0) + \frac{\mathrm{d}\tilde{\tau}_{\text{pass}}}{\mathrm{d}z'}(0)z' + \frac{1}{2}\frac{\mathrm{d}\tilde{\tau}_{\text{pass}}}{\mathrm{d}z'}(0)z'^2 + O(z'^2) \right), \tag{1.15}$$

where

$$\begin{aligned}
\tilde{\tau}_{\mathrm{pass}}(z')|_{z'=0} &= 2\frac{z'+h}{z'^2+2hz'+2h^2}\bigg|_{z'=0} = \frac{1}{h}, \\
\tilde{\tau}'_{\mathrm{pass}}(z')\big|_{z'=0} &= -2\frac{z'^2+2hz'}{(z'^2+2hz'+2h^2)^2}\bigg|_{z'=0} = 0, \\
\tilde{\tau}''_{\mathrm{pass}}(z')\big|_{z'=0} &= 4(z'+h)\frac{z'^2+2hz'-2h^2}{(z'^2+2hz'+2h^2)^3}\bigg|_{z'=0} = -\frac{1}{h^3}.
\end{aligned}$$

Eq. (1.15) becomes

$$\tau_{\mathrm{pass}}(z') \approx \frac{\mu b}{4\pi}\left(\frac{1}{h} - \frac{z'^2}{2h^3}\right) \ . \tag{1.16}$$

Parameter z' can be determine from the following idea. Brown approximates gently curved segments at the centre of the channel by circles with large radius of curvature r_{CD}. For the point $X[x', z']$ lying on the circle holds relation, see Fig. 1.3,

$$\begin{aligned}
x'^2 + (z' - r_{CD})^2 &= r_{CD}^2, \\
x'^2 + z'^2 - 2z'r_{CD} &= 0,
\end{aligned} \tag{1.17}$$

where x' measures the distance from the centre of the channel. While r_{CD} is large, $z'^2 \approx 0$ and curved screw dislocations have a position given by

$$z' \approx \frac{1}{2}\frac{x'}{r_{CD}} \ . \tag{1.18}$$

Finally, we find for the interaction stress

$$\tau_{\mathrm{pass}}(x') \approx \frac{\mu b}{4\pi h}\left(1 - \frac{x'^4}{8r_{CD}^2h^2}\right) \ , \tag{1.19}$$

and the average passing stress is given by

$$\langle\tau_{\mathrm{pass}}\rangle \approx \frac{\mu b}{4\pi h}\frac{2}{d_c}\int_0^{d_c/2}\left(1 - \frac{x'^4}{8r_{CD}^2h^2}\right)\mathrm{d}x' = \frac{\mu b}{4\pi h}\left(1 - \frac{d_c^4}{640r_{CD}^2h^2}\right) \ . \tag{1.20}$$

The radius of curvature at the centre of the channel is given by

$$\frac{T_{\mathrm{screw}}}{r_{CD}} = \tau^* b = (\tau - \tau_{\mathrm{pass}}(0))b = \left(\tau - \frac{\mu b}{4\pi h}\right) b \ . \tag{1.21}$$

If Eqs. (1.21), (1.20) and (1.13) are substituted into Eq. (1.12), we get an equation for the applied stress maintaining the dislocation in its position of unstable equilibrium:

$$\frac{2E_{\mathrm{edge}}}{bd_c} + \frac{\mu b}{4\pi h}\left(1 - \frac{b^2d_c^4}{640h^2T_{\mathrm{screw}}^2}\left(\tau - \frac{\mu b}{4\pi h}\right)^2\right)\left(1 - \frac{2T_{\mathrm{eff}}}{\tau b d_c}\right) = \tau \ . \tag{1.22}$$

Since Brown estimates $T_{\rm eff} \approx 0.1\mu b^2$ and $\mu \approx 10$ GPa, $b \approx 0.1$ nm, $d_c \approx 1\mu$m and with estimate, that $\tau \approx 10$ MPa, the final bracket differs negligibly from unity:

$$1 - \frac{2T_{\rm eff}}{\tau b d_c} \approx 1 - \frac{0.2\mu b}{\tau d_c} \approx 1 \ . \tag{1.23}$$

To solve Eq. (1.22) for τ let us consider that there exists a constant α such that

$$\tau - \frac{\mu b}{4\pi h} = \alpha \frac{2E_{\rm edge}}{b d_c} \ . \tag{1.24}$$

Using the Eq. (1.24) in Eq. (1.22), then α must satisfy the equation

$$\alpha^2 \frac{\mu b}{640\pi E_{\rm edge}} \left(\frac{d_c}{h}\right)^3 \left(\frac{E_{\rm edge}}{T_{\rm screw}}\right)^2 + \alpha - 1 = 0 \ . \tag{1.25}$$

It is easy to see from Eq. (1.25) if the screw tension is much greater than the edge energy, the screw dislocations are rigid and straight, giving $\alpha = 1$, and the flow stress is the simple addition of the passing stress and the Orowan bowing stress, as in Eq. (1.1). On the other hand, if the screw tension is much less than the edge energy the approximations cannot work. Brown shows[1] that the coefficient of α^2 in Eq. (1.25) to be about 2, which gives $\alpha \approx 0.5$. In fact, for values of the coefficient between 0.5 and 4, α varies slowly from 0.7 to 0.4. So it does not depend strongly upon the assumed values of the parameters.

Moreover, Brown shows that from Eq. (1.9) and the results of Mughrabi and Pschenitzka [**4**] we can calculate the value $\alpha = 0.17$.

If we write Eq. (1.25) in the form

$$\tau = \frac{2E_{\rm edge}}{b d_c} + \frac{\mu b}{4\pi h} - (1-\alpha)\frac{2E_{\rm edge}}{b d_c} = \tau_{\rm Orowan} + \tau_{\rm pass} \ , \tag{1.26}$$

we can recognise that the Orowan bowing stress must always be overcome, but the passing stress can be reduced from its value for infinite straight screw dislocations by bowing: the reduction amounting to some 50% of the Orowan stress. The main conclusion from model **Brown 2** is that the saturation stress is the sum of the bowing stress and the passing stress reduced from that for infinite straight screws. In summary: estimates of the factor α in Eq. (1.26) are $\alpha = 1$, Brown 1 [**3**], $\alpha = 0.17$, Mughrabi & Pschenitzka [**4**] and $\alpha = 0.5$, Brown 2 [**2**].

[1] Putting in values for copper, the ratio $E_{\rm edge}/T_{\rm screw} \approx 0.5$, the ratio $d/h \approx 30$, perhaps somewhat less.

Present Dislocation Model (Outline)

We propose a model to study the plasticity of single crystals by parametric dislocation dynamics using numerical simulations. The situation described correspond to the constrained glide of dislocations in the channels between the dislocation walls in persistent slip bands in fatigued metals, as studied analytically by Brown and Mughrabi & Pschenitzka.

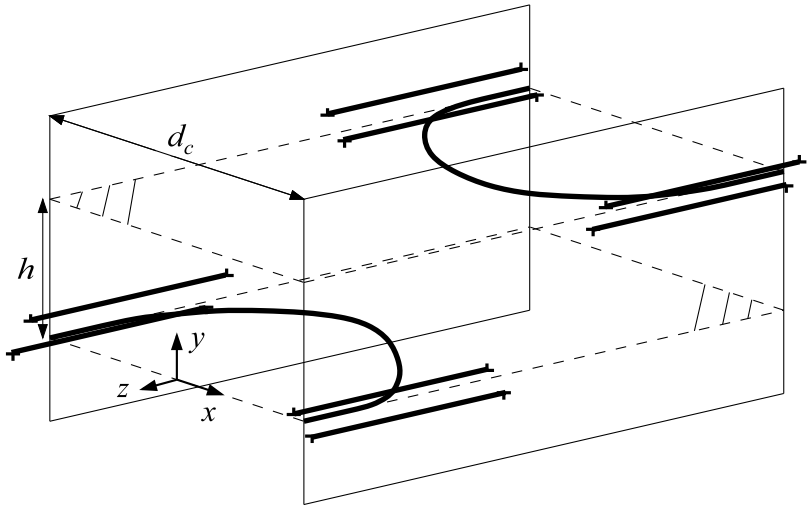

Figure 1.4: Geometry used in the DD simulations.

The geometry used in the dislocation dynamics simulations is schematically illustrated in Figs. 1.4 and 3.1.

Many previous analytical models use mathematical descriptions that apply only to straight, infinitely long dislocations and depend on assumptions as to what configurations dislocations will adopt. In our approach the gliding dislocations are considered flexible and finite. Initially they are kept apart in a straight screw position. The initial distance between dislocations is set up by the initial conditions. The boundary conditions are formulated in a such a way in order to simulate the depositing of dislocations in the walls of PSB channel.

As during simulation the dislocations are pushed by the applied stress between two walls, they attract one another and if their curvature is not great can be though of as forming dipole. Simultaneously each dislocation feels the elastic field by the nearest dislocation dipole in the walls.

The model includes the long-range character of the interaction among dislocations. We consider a linear relationship between the force acting on the gliding dislocation and the velocity magnitude. The slip force acting on a dislocation consists of resolved effective shear stress and the additional force caused by the flexibility of the dislocation line. In general, dislocation line will move if the slip force exceed the total friction force. Friction force consists of the lattice friction force and the resistance caused by the stored loops. But, in our model we neglected all the friction forces.

To estimate the distribution stress in the channel, two simplified limit cases are consider. In the first case the total stress is controlled, whereas in the second case the total shear strain is controlled. The reality is between these limit cases.

Dislocation dynamics simulations provide a better means to study dislocation interactions. The basic idea is to compute the forces on a dislocation arising from the applied stresses, from interactions with other dislocations, and from line tension effects. The dislocations are then moved in response to these forces. To the extent that the simulation is accurate, dislocation interactions and the evolution of dislocation structure can be simulated in a realistic way. One can then observe the configuration changes due to various dislocation interactions and compare the strengths of those interactions. These interactions often generate characteristic structures which can be identified experimentally to confirm the mechanisms.

Chapter 2

Relations for Dislocation Curves

To obtain the stress field produced by any dislocation, the theory of linear elasticity of dislocation was used. Due to strongly non-linear displacements close to the dislocation core, the model is not valid for this region. A basic feature common to most models, is that dislocations interact with each other through the long-range elastic stress field they produce in the host material.

2.1 Peach-Koehler Equation

The force per unit length exerted on an element of dislocation line which lies in the stress field τ_{ij} is given by the Peach-Koehler expression for force **[6, 7]**

$$f_i = \varepsilon_{ijk}\tau_{jm}b_m s_k \ . \tag{2.1}$$

Here f_i is the i-th component of the interaction force per the unit length of the dislocation line, ε_{ijk} Levi-Civita symbol[1], τ_{jm} components of the stress field tensor at the dislocation position, b_m components of the Burgers vector $\mathbf{b}$ and s_k denote components of unit vector $\mathbf{s}$ which has the direction of the dislocation line.

The Eq. (2.1) written in the vector notation

$$\mathbf{F} = (\tilde{\tau}\mathbf{b}) \times \mathbf{s} \ , \tag{2.2}$$

where $\tilde{\tau}$ is the stress tensor. The symbol '$\times$' stands for the cross product of vectors. According to Eq. (2.2) force acting on an element of dislocation line is always perpendicular to dislocation line.

[1] $\varepsilon_{ijk} = 1$ if (i, j, k) are in cyclic order; 0 if any of (i, j, k) are equal; -1 if (i, j, k) are in acyclic order.

Peach-Koehler Eq. (2.1) is valid also in the case when τ_{ij} is the stress generated from different kind of defects, for example by another dislocation line.

2.2 Stress Field of a Dislocation Segment

The direction of a straight dislocation segment is given by a constant unit vector $\mathbf{s}'$. The parametric vector equation for this segment can be written

$$\mathbf{r}' = \mathbf{a}' + p'\mathbf{s}', \tag{2.3}$$

where $\mathbf{a}'$ is a constant vector and p' a real variable. A field point may be given by the positional vector $\mathbf{r}$, Fig. 2.1. Radius vector $\mathbf{R}$ from the primed point on the curve to the unprimed field point is

$$\mathbf{R} = \mathbf{r} - \mathbf{r}'. \tag{2.4}$$

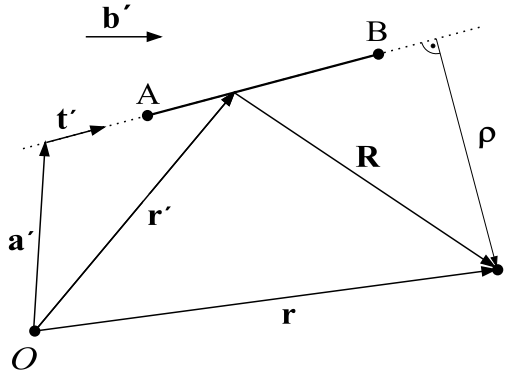

Figure 2.1: Dislocation segment AB exerts on a field point $\mathbf{r}$.

Further, we define q as the integral taken along the dislocation line, $q = \int_{-\infty}^{+\infty} R \, \mathrm{d}p'$, which is

$$q = \frac{1}{2}\varrho^2 \left[\ln(L' + R) - \frac{1}{2}\right] - \frac{1}{2}L'R \ , \tag{2.5}$$

where R is the magnitude of the radius vector, ϱ is the magnitude of the distance vector $\vec{\varrho}$ from the dislocation, $\vec{\varrho} = \mathbf{R} - L'\mathbf{s}'$. $L' = \mathbf{R} \cdot \mathbf{s}'$ is the projection of the vector $\mathbf{R}$ to the dislocation line, Fig. 2.1. The dot '$\cdot$' stands for the scalar product of vectors.

By the differentiating (2.5) with respect to x_i, x_j and x_m, respectively, we find

$$\begin{aligned} q_{,ij} &= -(\delta_{ij} - s'_i s'_j)\ln(L'+R) - \frac{\varrho_i s'_j + \varrho_j s'_i + L' s'_i s'_j}{R} \\ &\quad - \frac{\varrho_i \rho_j}{R(L'+R)}, \qquad (2.6) \\ q_{,ijm} &= -\frac{\delta_{im}P_j + \delta_{jm}P_i + \varrho_m(\delta_{ij} - s'_i s'_j)}{R(L'+R)} - \frac{\varrho_i s'_j + \varrho_j s'_i + L' s'_i s'_j}{R^3}\varrho_m \\ &\quad - \frac{\varrho_i \varrho_j (L'+2R)}{R^3(L'+R)^2}\varrho_m, \qquad (2.7) \end{aligned}$$

where P_i and P_j are the components of the vector $\mathbf{P} = \mathbf{R} - R\mathbf{s}'$, s'_i and s'_j are components of the vector $\mathbf{s}'$, ϱ_i, ϱ_j and ϱ_m components of the vector $\vec{\varrho}$. δ_{ij} is Kronecker delta[2].

According to de Wit [**8**] the stress tensor components τ_{ij} generated at a point $\mathbf{r}$ by the semi-infinite straight dislocation of Burgers vector $\mathbf{b}'$ and the line direction $\mathbf{s}'$ are given by

$$\tau_{ij} = \frac{\mu b'_n}{8\pi}\left[q_{,mll}\left(\varepsilon_{jmn}s'_i + \varepsilon_{imn}s'_j\right) + \frac{2}{1-\nu}\varepsilon_{kmn}\left(q_{,mij} - q_{,mll}\delta_{ij}\right)s'_k\right]. \qquad (2.8)$$

The usual summation convention over repeated indices is employed. The symbols following the primes in the sub index refer to spatial derivation. μ is the shear modulus, ν Poisson ratio, ε_{ijk} Levi-Civita symbol and δ_{ij} Kronecker delta. Next, b'_n is the component of the Burgers vector $\mathbf{b}'$, s'_i, s'_i and s'_k are components of the line direction $\mathbf{s}'$ and the quantity $q_{,ijk}$ is given by equation (2.7).

The expression (2.8) for the stress tensor σ_{ij} in general tensor notation with respect to an arbitrary Cartesian coordinate system:

$$\begin{aligned} \tau_{ij}(\mathbf{R}) &= \frac{\mu}{4\pi}\frac{1}{R(R+L')}\left\{(\mathbf{b}\times\mathbf{P})_i s'_j + (\mathbf{b}\times\mathbf{P})_j s'_i - \frac{1}{1-\nu}\left((\mathbf{b}\times\mathbf{s}')_i P_j + \right.\right. \\ &+ \left.\left.(\mathbf{b}\times\mathbf{s}')_j P_i\right) - \frac{(\mathbf{b}\times\vec{\varrho})\cdot\mathbf{s}'}{1-\nu}\left[\left(\varrho_i s'_j + \varrho_j s'_i + L' s'_i s'_j\right)\frac{R+L'}{R^2} + \right. \\ &+ \left.\left.\delta_{ij} + s'_i s'_j + \varrho_i\varrho_j\frac{2R+L'}{R^2(R+L')}\right]\right\}. \qquad (2.9) \end{aligned}$$

Finally, the stress field of a dislocation segment lying between the points [3] A and B on the infinite dislocation line one obtains by subtracting the solutions

[2] $\delta_{ij} = 1$ if $i = j$; 0 otherwise

[3] Vectors $\vec{AB}$ and $\mathbf{s}'$ has the same direction.

of the Eq. (2.9) at these two points, see Fig. 2.1, with respect to an arbitrary Cartesian coordinate system is:

$$\sigma_{ij}^{(AB)} = \sigma_{ij}\left(\mathbf{R}_B\right) - \sigma_{ij}\left(\mathbf{R}_A\right) \ . \tag{2.10}$$

Finally recall the expression for the stress around edge dislocation. Consider a Cartesian coordinates. The shear stress σ_{xy} exerted at a point (x, y, z) by an edge dislocation located at the origin is

$$\sigma_{xy} = \frac{Ax(x^2 - y^2)}{(x^2 + y^2)^2} \ , \tag{2.11}$$

where $A = \mu b/2\pi(1 - \nu)$ is a coefficient involving the shear modulus μ, the Poisson's ration ν and the magnitude b of the Burgers vector.

Chapter 3

Boundary Conditions

The studied volume is supposed to represent part of a real crystal, which we present as continuum.

Fig. 3.1 shows the situation in the PSB channel in more details in the opposite direction than the orientation of the z axis of the **main** coordinates system. The origin is set up in the middle of the channel in the first slip plane. We consider two perfect dislocations in crystal with Burgers vector $\mathbf{b}$, which is oriented in the x direction. The two dislocations (Γ_1 and Γ_2) of opposite sign glide in parallel planes (the 1^{st} and the 2^{nd}, respectively), with a spacing h and in a channel of width d_c. The slip planes are parallel to xz-plane.

We consider that the interaction between the walls of the PSB channel and the gliding dislocations is elastic. In the proposed theoretical model, the walls consists of many dislocation dipoles. Each gliding dislocation feels strongly the elastic field only from the nearest dislocation dipole in each wall, see Fig. 1.4.

3.1 Dislocation Dipole

A dislocation dipole is formed by the two infinitely long straight edge dislocations of opposite sign[1]. Their stress field are superimposed. In this case, the stresses are reduced. Introduce notation: $\mathbf{b}_2$ is the Burgers vector in the direction of the x axis in the main coordinates system, $\mathbf{b}_1$ with the opposite orientation and naturally $b = b_1 = b_2$, see Fig. 3.1.

[1]The sense of the Burgers vector defines the sign of the edge dislocation if not specify otherwise.

Each edge dislocation has Burgers vector parallel to x axis and its direction point to out of the wall, see Fig. 3.1.

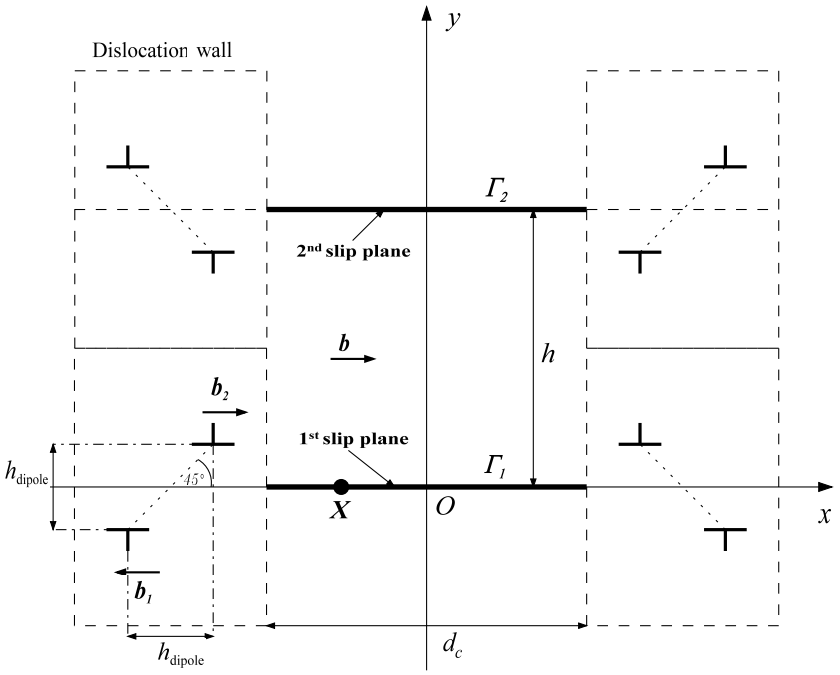

Figure 3.1: Geometry of dipolar dislocation walls

3.2 Dislocation Walls

We assume that the dislocation walls are formed by the edge infinitely long dislocation dipoles. We assume rigid dipoles, of vacancy type, each held in two possible equilibrium configurations oriented either $45°$ or $-45°$ with respect to the slip planes. Each dipole is parallel to the z axis, as shown in Fig. 3.1. The midpoint[2] of each such dipole lies either on the 1^{st} or the 2^{nd} slip plane. We assume that during simulations the dipoles has stable position and they are not allow to move.

The magnitude of the stress generated by the dipoles is controlled by its height h_{dipole}. The stress acting on the point $X[x, 0, z] \in 1^{\text{st}}$ *slip plane* from

[2]They are not indicated in Fig. 3.1

the dipole on the left hand side is:

$$\tau_{\text{wall}} = \sigma_{xy} = \frac{\mu b}{2\pi} \frac{1}{1-\nu} \left(-\frac{x_1 \left(x_1^2 - y_1^2\right)}{\left(x_1^2 + y_1^2\right)^2} + \frac{x_2 \left(x_2^2 - y_2^2\right)}{\left(x_2^2 + y_2^2\right)^2} \right) , \tag{3.1}$$

where x_i and y_i are components of the radius vector $\mathbf{R}_i$ between the field point X and the edge dislocation with Burgers vector $\mathbf{b}_i$, $i = 1, 2$, forming the dislocation dipole, Fig. 3.1. Similar relation holds for the stress by the dipole on the right hand side:

$$\tau_{\text{wall}} = \sigma_{xy} = \frac{\mu b}{2\pi} \frac{1}{1-\nu} \left(\frac{x_1 \left(x_1^2 - y_1^2\right)}{\left(x_1^2 + y_1^2\right)^2} - \frac{x_2 \left(x_2^2 - y_2^2\right)}{\left(x_2^2 + y_2^2\right)^2} \right) , \tag{3.2}$$

with the same meaning of x_i and y_i as above. Note, that the stresses generated by the dipole on the right hand side and on the left hand side are identical. Resulting stress field by the walls acting at the field point X is a sum of the stress fields produced by these two dipoles. The Fig. 3.2 shows a two-dimensional plots of the shear stress[3] given by Eq. (3.1) as a function of a coordinate x_{wall} in the 1st slip plane along the x axis with respect to the midpoint of the dipole.

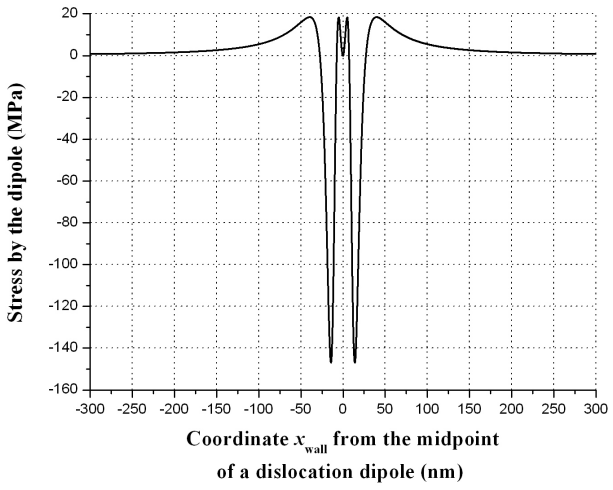

Figure 3.2: Stress by the dislocation dipole in the wall.

[3]With parameters $h_{\text{dipole}} = 20$ nm, $b = 0.25$ nm, $\mu = 42,1$ GPa, $\nu = 0.43$.

Choice of parameters

The height of the dislocation dipoles is consider to be $h_{\text{dipole}} = 20$ nm. Note that critical spacing for annihilation of edge dislocations of opposite sign is about 46 nm, Brown [**2**]. Value of h_{dipole} was chosen in this way that we can vary the applied stress in interval $0 - 100$ MPa for all numerical simulations.

The corner points of each dislocation curve are initially distant from the midpoint of the nearest dipole 25 nm. Following Fig. 3.1, the end points of the curves are fix in the z component. Since we assume the motion only in the planes parallel to xz-plane, just x component of these points can vary in time. So as the dislocation segment bow out and advances, its length increases and the distance of the edge parts of the dislocation deposited at the walls of the channel are determined by the stress from dipoles and effective stress.

Chapter 4

Dislocation Dynamics

4.1 Basic Equation of Motion

A linear relationship between the forces acting on a curved dislocation and the magnitude of the velocity is consider. The crystallographic glide of the planar dislocation segments in the crystal can be assumed to be govern by a linear viscous law of the kind (so called mean curvature flow equation [**9**])

$$Bv = \kappa T + F_{\text{eff}}. \tag{4.1}$$

Here, B is the phonon drag coefficient, v is the magnitude of the normal velocity of the evolving curve. The first term on the right-hand side which represents the self force is expressed in the line tension approximation as the product of the line tension T by the local curvature κ. F_{eff} represents the magnitude of the local driving force acting on the dislocation segment at given position and time.

4.2 Forces Acting on the Dislocation

In general, the effective force $\mathbf{F}_{\text{eff}}$ is a sum of several contributions: external (applied) force $\mathbf{F}_{\text{app}}$ resolved in the glide plane; interaction force $\mathbf{F}_{\text{disl}}$ incorporates the interactions with another dislocation curve; $\mathbf{F}_{\text{wall}}$ from dislocation dipoles representing walls; $\mathbf{F}_{\text{loop}}$ is the interaction force between the dislocation curve and dipolar loops and the friction force $\mathbf{F}_{\text{fri}}$:

$$\mathbf{F}_{\text{eff}} = \mathbf{F}_{\text{app}} + \mathbf{F}_{\text{disl}} + \mathbf{F}_{\text{wall}} + \mathbf{F}_{\text{loop}} + \mathbf{F}_{\text{fri}} \ . \tag{4.2}$$

In our model we neglected the last two contributions.

The equation (4.1) is set up by balancing the force acting on the dislocation. Here, we get detailed knowledge of the terms in the Eq. (4.2).

4.2.1 Effective Force

As the dislocation is allowed to move in the plane parallel to xz-plane, we need to express f_x and f_z from the Peach-Koehler equation. f_x and f_z are the first and the third component of the effective force. We assume, that Burgers vector has the same direction as x-axis of the main coordinate system, $\mathbf{b} = [b, 0, 0]$, $b > 0$. Then we have

$$f_x = \sigma_{xy} b s_z, \quad f_z = -\sigma_{xy} b s_x, \tag{4.3}$$

where $\tau_{\text{eff}} \equiv \tau_{xy}$ is the effective resolved shear stress acting on the segment in the glide plane. s_x and s_z are the components of the dislocation curve's tangential vector $\mathbf{X}_s$:

$$\mathbf{X}_s = [s_x, 0, s_z] \equiv [X_s^x, 0, X_s^z] \ .$$

From Eqs. (2.2) and (4.3) it follows that the effective force acting at given position of the dislocation curve is perpendicular to the dislocation line $\Gamma(t)$ and can be express as

$$\begin{aligned} \mathbf{F}_{\text{eff}} &= \tau_{\text{eff}} b \mathbf{X}_s^{\perp} = \\ &= (\tau_{\text{app}} + \tau_{\text{disl}} + \tau_{\text{wall}} + \tau_{\text{loop}} + \tau_{\text{fri}})\, b \mathbf{X}_s^{\perp}, \end{aligned} \tag{4.4}$$

with

$$\mathbf{X}_s^{\perp} = [X_s^z, 0, -X_s^x]. \tag{4.5}$$

Since we use the elastic small strain linear theory the local resolved effective shear stress is a sum of several contributions: τ_{app} corresponds to the applied shear stress resolved in the slip plane; τ_{disl} incorporates the interaction with the another gliding dislocation lines; τ_{wall} covers the stress from the stable dipoles in the walls of the PSB channel; τ_{loop}, if there are some dislocation loops in the channel; τ_{fri}, a lattice friction or Peierls stress τ_{Peierls} which is a small fraction of the shear modulus μ. (for example, for Cu monocrystal one estimates $\tau_{\text{Peierls}} = 3 \times 10^{-5}\mu = 1,26$ MPa [**10**]). In our approach we neglected this contribution to the effective stress.

4.2.2 Interaction Stress

The elastic field of a curved dislocation can be expressed as

$$\tau_{\text{disl}}(t) = \int_{\Gamma(t)} \mathrm{d}\tau_{\text{disl}}, \tag{4.6}$$

where the integral taken along the curve Γ at time t corresponds to a synthesis of the elastic fields $\mathrm{d}\tau_{\text{disl}}$ generated by the dislocation elements $\mathrm{d}s$ of the curve. $\tau_{\text{disl}}(t)$ is a stress field by a dislocation curve $\Gamma(t)$ with respect to given point.

4.3 Line Tension

The concept of line tension, or self stress of the dislocation line, is the key feature in our approach. The curved dislocation feels its own elastic field of as a straightening force, which can be expressed conveniently in the line tension approximation, DeWitt and Koehler [**11**]. For us, the important characteristic of the line-tension approximation is that this force locally points in the direction opposing the direction of maximal possible increase in the line length when the dislocation moves.

Energy per unit length of the dislocation is $E(\alpha) = E_{\text{edge}}\,(1 - \nu\cos^2(\alpha))$, where ν is Poisson's ratio and E_{edge} is the line energy of a dislocation in the edge orientation and is given by relation (1.3). The angle α is angle between Burgers vector and the tangent to the dislocation line at given position and time. The line tension depend on the character of the dislocation [**12**]:

$$T(\alpha) = E + \frac{\partial^2 E}{\partial \alpha^2} = E_{\text{edge}}\left(1 - 2\nu + 3\cos^2(\alpha)\right). \tag{4.7}$$

Especially

$$T_{\text{screw}} = E_{\text{edge}}(1+\nu), \tag{4.8}$$

$$T_{\text{edge}} = E_{\text{edge}}(1-2\nu). \tag{4.9}$$

The straightening force per unit length $F_{\text{own}} = b\tau_{\text{own}} = \kappa T(\alpha)$ approximates the self force due to the short-range stress field of the individual dislocation. κ is the local curvature of dislocation.

4.4 Damping Dislocation Glide

A drag coefficient is caused by interactions with phonons. Values which were experimentally measured at room temperature: $B = 1.5 \times 10^{-5}$ Pa·s for Copper, [**13**], $B = 1.0 \times 10^{-5}$ Pa·s for Nickel, [**14**]. In the present work we analyze the case that B is a constant given by material. A drag coefficient is in general orientation depended, but in the present model this dependences will be neglected.

4.5 Stress Distribution in the Channel

The glide dislocations are moved by the shear stress resolved in the slip planes. Instead of solving rather difficult full two or three dimensional problem of the stress distribution in the channel two simplified limit cases are

consider, Fig. 4.1. The first case describes an uniform stress in the channel and the second the case of homogeneous total shear strain. The reality is between these two limit cases. The former case gives upper stress bound, the latter case lower stress bound of the endurance limit.

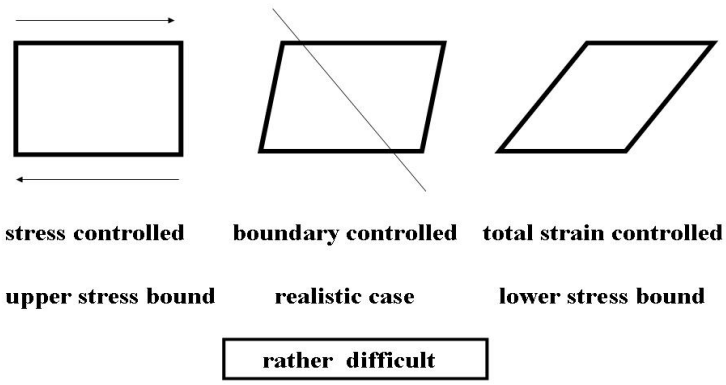

Figure 4.1: Stress and total strain controlled.

4.5.1 The Uniform Applied Stress

In that case the applied force is the same in each point of the dislocation line. In our numerical simulations the applied stress can be, in general, an arbitrary function of time. The magnitude of the force per unit length on the gliding dislocation is represented by a term $b\tau_{\text{app}}$, where τ_{app} is applied stress and b is the magnitude of the Burgers vector:

$$F_{\text{app}} = b\tau_{\text{app}}. \tag{4.10}$$

Especially, for the numerical simulations we assume a special case when applied stress τ_{app} is independent of time and homogenous through the channel (creep test):

$$\tau_{\text{app}} = \text{const.} \tag{4.11}$$

4.5.2 The Homogeneous Total Shear Strain

It is supposed that the total shear strain ε_{tot}, as a sum of the elastic and plastic part

$$\varepsilon_{\text{tot}} = \varepsilon_{\text{elas}} + p, \tag{4.12}$$

is homogeneous in the channel. For the simplicity elastic homogeneity and isotropy is supposed.

Between an applied stress τ_{app} and an elastic shear strain $\varepsilon_{\text{elas}}$ hold linear relationship (Hooke's law)

$$\varepsilon_{\text{elas}}(\mathbf{X}, t) = \frac{\tau_{\text{app}}(\mathbf{X}, t)}{\mu}, \tag{4.13}$$

where μ is the shear modulus, t time and $\mathbf{X}$ specify a position in the channel.

If ϱ denote the constant scalar density of the mobile dislocations, $v(\mathbf{X}, t)$ velocity of a dislocation at the fix point $\mathbf{X}$ on the dislocation, t time and b magnitude of the Burgers vector $\mathbf{b}$, the rate of the plastic shear strain $p(t)$ is given by the Orowan equation [1] $\dot{p}(\mathbf{X}, t) = \varrho b v(\mathbf{X}, t)$, hence

$$p(\mathbf{X}, t) = \varrho b \int_{t_0}^{t} v(\mathbf{X}, t) \mathrm{d}t. \tag{4.14}$$

$t_0 = 0$ is a time such that $\varepsilon_{\text{tot}}(\mathbf{X}, t_0) = 0$ for all points $\mathbf{X}$ on the curve. A suitable relationship for plastic part is also

$$p(t)l(t) = \varrho b \int_{l} \int_{t_0}^{t} v(\mathbf{X}, t) \mathrm{d}t \mathrm{d}s = \varrho b S(\mathbf{X}, t), \tag{4.15}$$

where we integrate along an infinitesimal straight segment $l(t)$ containing the point $\mathbf{X}$. $S(t)$ correspond to slipping area by the infinitesimal straight element l in time interval (t_0, t). The shear stress applied to the dislocation can be expressed as

$$\tau_{\text{app}}(t)l(t) = \mu \varepsilon_{\text{tot}}(t)l(t) - \mu \varrho b S(t), \tag{4.16}$$

where $l(t)$ is the length of an infinitesimal straight segment at time t.

Especially, let the total shear strain ε_{tot} be a linear function of time (tension test):

$$\varepsilon_{\text{tot}}(t) = \varepsilon t. \tag{4.17}$$

[1] $\dot{p}(\mathbf{X}, t)$ means partial derivation with respect to time.

Chapter 5

Mathematical Models of a Dislocation

At the micro scale we can describe a dislocation line as a curve. The motion of the dislocation line then correspond to the evolution of the curve.

In the previous chapter, Eq. (4.1), we recall the mean curvature flow equation which govern evolution of the dislocation curve. To solve our problem we use the parametric approach [**15**]. However we briefly introduce two other possible methods for comparison: the description as a graph [**16, 17, 18**] and the level set method [**16, 17, 18**]. In all cases we derive a partial differential equation (PDE) of a type of the diffusion equation.

5.1 Parametric Approach

In the parametric method the gliding dislocation curve $\Gamma(t)$ at time t can be described by a smooth time dependent vector function $\mathbf{X}(S, I)$

$$\mathbf{X} : S \times I \to \mathbb{R}^2, \tag{5.1}$$

where $S = [a, b]$ is a fixed parameterization interval and $I = [0, T)$, $T > 0$, is a time interval. It means that for any time $t \in [0, T)$ the dislocation curve is given as

$$\Gamma(t) = \text{Image}(\mathbf{X}(\cdot, t)) = \{\mathbf{X}(u, t), u \in S\}, \tag{5.2}$$

where $u \in S$ is a parameter.

Since dislocations move along crystallographic planes we assume that set $\{\mathbf{X}(u, t), u \in S\}$ is the subset of the plane in the Cartesian coordinate system for any time $t \in I$.

Arc Length Parameterization

Consider a smooth curve, $|\mathbf{X}_u| > 0$, for all $u \in S$ and for any time t. Here $|\mathbf{X}_u|$ denote Euclidean norm of the vector $\mathbf{X}_u$.

Vectors tangent and normal to the dislocation line (in the glide plane) are $\mathbf{X}_u = \partial_u \mathbf{X}$ and $\mathbf{X}_u^\perp$, respectively. Moreover, the outward normal vector $\mathbf{X}_u^\perp$ is given by the condition $\det(\mathbf{X}_u, \mathbf{X}_u^\perp) = 1$. Symbol $(\mathbf{a}, \mathbf{b})$ mean 2×2 matrix with column vectors $\mathbf{a}$ and $\mathbf{b}$.

The unit arc length parameterization will be denoted by s. Then a line element $\mathrm{d}s$ of the curve $\Gamma(t)$ is $\mathrm{d}s = |\mathbf{X}_u| \, \mathrm{d}u$. Let be $u_0 \in S$ an arbitrary fixed point in the interval S. The distance $s(u,t)$ measured along the curve from the point $\mathbf{X}(u_0, t)$ to the point $\mathbf{X}(u,t)$, $u > u_0$, is

$$s(u,t) = \int_{u_0}^{u} |\mathbf{X}_u(u',t)| \, \mathrm{d}u'. \tag{5.3}$$

As the distance s is a growing function of u, an inverse function $u = u(s)$ exists. The natural parameterization of the dislocation $\mathbf{X}(u,t)$ by the distance $s(u,t) \in \langle 0, L(t) \rangle$ is $\mathbf{X}(s,t) \equiv \mathbf{X}(u(s),t)$. We denote $L(t)$ the total length of the dislocation curve $\Gamma(t)$ at the time t.

Note that $\mathbf{X}_s$ and $\mathbf{X}_s^\perp$ represent unit tangent and normal vectors, respectively. It is clear from formally written equations

$$\mathbf{X}_s = \mathbf{X}_u \frac{\mathrm{d}u}{\mathrm{d}s} = \mathbf{X}_u \frac{\mathrm{d}u}{|\mathbf{X}_u| \, \mathrm{d}u} = \mathbf{X}_u / |\mathbf{X}_u| \,,$$

where we use fact that for arc length parameterization s is $\mathrm{d}s = |\mathbf{X}_u| \, \mathrm{d}u$.

Governing Equation

Here we point to the full differential equation which govern the gliding dislocation curve in the parametric approach, see Eq. (4.1).

For the magnitude of the normal component v of the velocity holds

$$v = \partial_t \mathbf{X} \cdot \mathbf{n}_\Gamma = \mathbf{X}_t \cdot \mathbf{X}_s^\perp. \tag{5.4}$$

The dot '$\cdot$' stands for the scalar product of vectors. The curvature $\kappa = \kappa(u,t)$ of the curve at u is defined through the Frenet's formula

$$\partial_s \mathbf{X}_s = \kappa \mathbf{X}_s^\perp. \tag{5.5}$$

In the Eqs. (5.4) and (5.5) s denote the arc length parameterization. The next step is to multiply Eq. (5.5) through by unit normal vector $\mathbf{X}_s^\perp$. We get

for the local curvature equation

$$\kappa = \mathbf{X}_{ss} \cdot \mathbf{X}_s^{\perp}. \tag{5.6}$$

The external driving force $\mathbf{F}_{\text{eff}}$ has the same direction as the normal vector of the curve, so its magnitude F_{eff} can be express as

$$F_{\text{eff}} = F_{\text{eff}} \mathbf{X}_s^{\perp} \cdot \mathbf{X}_s^{\perp}. \tag{5.7}$$

Then the Eq. (4.1) can be rewritten, with help of the Eqs. (5.4), (5.6) and (5.7), to the form $B\mathbf{X}_t \cdot \mathbf{X}_s^{\perp} = \mathbf{X}_{ss} \cdot \mathbf{X}_s^{\perp} + F_{\text{eff}} \mathbf{X}_s^{\perp} \cdot \mathbf{X}_s^{\perp}$.

We are now in a position to make the final argument. For a vector $\mathbf{a}$ and a unit vector $\mathbf{n}$ the expression $(\mathbf{a} \cdot \mathbf{n}\,)\,\mathbf{n}$ gives the projection of the vector $\mathbf{a}$ in the direction of the unit vector $\mathbf{n}$. For this reason the last equation has the form of intrinsic diffusion equation

$$B\mathbf{X}_t = T\mathbf{X}_{ss} + F_{\text{eff}} \mathbf{X}_s^{\perp} \tag{5.8}$$

for the position vector $\mathbf{X}$ at given position and time.

5.2 Description of the Dislocation Curve as a Graph

We assume that the gliding dislocation curve $\Gamma(t)$ at time t can be written in the form

$$\Gamma(t) = \{(x, g(x,t)) : x \in \Omega)\},$$

where $\Omega \subset \mathbb{R}$ is interval and the function $g : \Omega \times [0, T) \to \mathbb{R}$ has to be found.

The normal vector $\mathbf{n}_\Gamma$ in the glide plane of the curve $\Gamma(t)$ at a point $(x, g(x,t))$ is given by

$$\mathbf{n}_\Gamma = \frac{(\nabla_x g, -1)}{\sqrt{1 + |\nabla_x g|^2}}. \tag{5.9}$$

Since only normal component v of the velocity determines the evolution of the curve, we get

$$v = (\dot{x}, \partial_t g) \cdot \frac{(\nabla_x g, -1)}{\sqrt{1 + |\nabla_x g|^2}} = -\frac{\partial_t g}{\sqrt{1 + |\nabla_x g|^2}}, \tag{5.10}$$

since $\dot{x} \equiv \mathrm{d}x/\mathrm{d}t = 0$.

The mean curvature κ is given by $\kappa = \operatorname{div} \mathbf{n}_\Gamma$, i.e.

$$\kappa = \nabla_x \cdot \left(\frac{\nabla_x g}{\sqrt{1 + |\nabla_x g|^2}} \right). \tag{5.11}$$

Eq. (4.1) then leads to the partial differential equation (PDE)

$$-\frac{B\partial_t g}{\sqrt{1 + |\nabla_x g|^2}} = \nabla_x \cdot \left(\frac{\nabla_x g}{\sqrt{1 + |\nabla_x g|^2}} \right) T + F_{\text{eff}}. \tag{5.12}$$

Here B is a drag coefficient, T denote the line tension and F_{eff} the effective force acting on the curve.

The corresponding PDE has a formal similarity to a regularized version of the level set PDE.

This approach was used in the previous work [**19, 20**].

5.3 Level Set (Eulerian) Method

Level set (or so-called Eulerian) approach simplicity handles the motion by passing the problem to a higher dimensional space and solving there the evolution equation for a graph whose evolving level sets correspond to the evolving curve or surface.

One looks for $\Gamma(t)$ as the zero level set of an auxiliary function $P(\mathbf{g}(t), t) : \mathbb{R}^{n+1} \times [0, \infty) \to \mathbb{R}$, $(n = 1)$, of class C^2, for which the moving curve $\mathbf{g}$ is the same level line at each time moment t, i.e.

$$\Gamma(t) = \left\{ \mathbf{g} \in \mathbb{R}^{n+1} : P(\mathbf{g}(t), t) = 0 \right\} \tag{5.13}$$

for every $t \in I = [0, T)$, $T > 0$. Contrary to parametric and graph approach, the level set method is capable of tracking topological changes of $\Gamma(t)$ (like pinching-off or merging). This advantage, however, needs to be offset against the fact that the problem now becomes $(n + 1)$-dimensional in space.

Since $P(\mathbf{g}, t)$ is equal to 0, differentiating (5.13) in time one gets

$$\partial_t P(\mathbf{g}, t) + \nabla_{\mathbf{g}} P(\mathbf{g}, t) \cdot \mathbf{g}'(t) = 0. \tag{5.14}$$

As in previous section, only normal component v of the velocity determines the evolution of the curve, hence

$$v = \mathbf{g}'(t) \cdot \mathbf{n}_\Gamma. \tag{5.15}$$

where $\mathbf{n}_\Gamma = \nabla_{\mathbf{g}} P / |\nabla_{\mathbf{g}} P|$ is the outer normal vector to the level line of P. Using (5.15) in (5.14) we obtain the Hamilton-Jacobi partial differential equation (Evans), [**9, 17, 18**]:

$$\partial_t P(\mathbf{g}, t) + v \, |\nabla_{\mathbf{g}} P(\mathbf{g}, t)| = 0 \tag{5.16}$$

for unknown function P. From relation $\kappa = \operatorname{div} \mathbf{n}_\Gamma$ which holds for the curvature κ of the level set line of P passing through point $\mathbf{g}$, we get from (5.16) and (4.1) the level set equation

$$B \; \partial_t P = |\nabla_{\mathbf{g}} P| \, \nabla_{\mathbf{g}} \cdot \left(\frac{\nabla_{\mathbf{g}} P}{|\nabla_{\mathbf{g}} P|} \right) T + |\nabla_{\mathbf{g}} P| \, F_{\text{eff}}, \tag{5.17}$$

where B is a drag coefficient, T is a line tension and F_{eff} is the effective force. The law (4.1) now translates into a nonlinear, parabolic degenerate and singular PDE for P (Lions), [**9, 18**]. The equation should be accompanied by a boundary conditions and initial condition.

Eq. (5.17) is not defined where the gradient of P vanishes. But sets where $\nabla_{\mathbf{g}} P = 0$ are of interest for us, since typically here the topology of Γ changes. Thus one needs an appropriate notion of solution for (5.17).

Chapter 6

Governing Equations

The general mathematical model consists of the two equations of motion, one for each gliding dislocation, including suitable boundary and initial conditions.

$$B\mathbf{X}_t = T\mathbf{X}_{ss} + F_{\text{eff}}\mathbf{X}_s^{\perp} \tag{6.1}$$

for curve Γ_1 and

$$B\mathbf{Y}_t = \tilde{T}\mathbf{Y}_{ss} + \tilde{F}_{\text{eff}}\mathbf{Y}_s^{\perp} \tag{6.2}$$

for curve Γ_2. T and $\tilde{T}$ are line tensions at given position and time. F_{eff} and $\tilde{F}_{\text{eff}}$ are magnitudes of effective forces acting on the curve Γ_1 at $\mathbf{X}$ and on the curve Γ_2 at $\mathbf{Y}$, respectively. The initial shape of each glide dislocation at time $t = 0$ has a form of straight dislocation segment (in a screw configuration). The direction of a curve Γ_1 is chosen in the direction of the x-axis of main coordinate system, direction of a curve Γ_2 in the opposite direction. The boundary conditions has been specified in Section 3.2.

The expressions for the stress field by the dipoles forming the dislocation walls is given by Eqs. (3.1) and (3.2), the stress field of a gliding dislocation is given by Eq. (4.6). Finally, in case when applied stress is controlled, τ_{app} satisfied Eq. (4.11); when the total shear strain is controlled, τ_{app} satisfied Eq. (4.16).

Chapter 7

Numerical Scheme

The system of equations (6.1) and (6.2) is too complicated to be solved analytically, however, it is suitable for numerical simulation of the motion of the glide dislocations. For computer simulations of the problem described in previous chapter we use flowing finite volume method [**21**] in space and the method of lines [**22**] in time.

7.1 Discretization of the Curve

In general, each discrete solution is represented by a moving polygon given, at any time $t \in (0, T)$, by plane points. The dislocation curve is discretized in the arc length parameterization s; points of the curve are denoted by sub index i, Fig. 7.1:

$$\begin{aligned} \mathbf{X}_i &= \mathbf{X}_i(t) = \mathbf{X}(s_i, t), \quad i = 0, \ldots, M, \\ 0 &= s_0 < s_1 < \ldots < s_M = L(t), \end{aligned}$$

where $L(t)$ is the total length of the dislocation curve $\Gamma(t)$ at the time t . $M \in \mathbb{N}$ is a natural number which determine the number of points on the curve. X_i^x, X_i^y and X_i^z are the components of the point $\mathbf{X}_i$ in Cartesian coordinate system.

Smooth curve is approximate by M linear segments $[\mathbf{X}_{i-1}, \mathbf{X}_i]$ called flowing finite volumes, $i = 1, \ldots, M$. For our own use we construct also dual volumes $\mathcal{V}_i = \left[\mathbf{X}_{i-1/2}, \mathbf{X}_i\right] \cup \left[\mathbf{X}_i, \mathbf{X}_{i+1/2}\right]$, $i = 1, \ldots, M-1$. Here the point $\mathbf{X}_{j+1/2}$ is a midpoint of the line segment $\mathbf{X}_j\mathbf{X}_{j+1}$, i.e. $\mathbf{X}_{j+1/2} = \frac{1}{2}(\mathbf{X}_j + \mathbf{X}_{j+1})$, $j = 0, \ldots, M-1$.

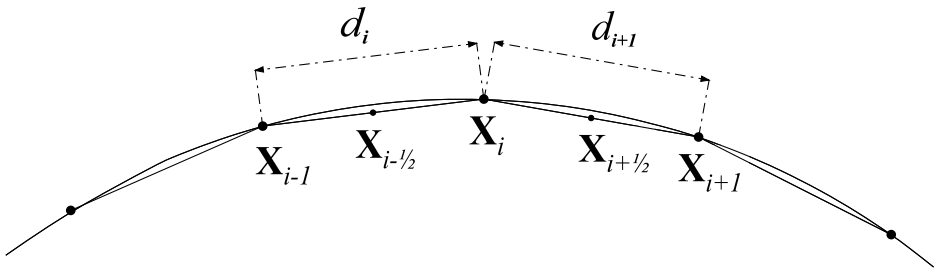

Figure 7.1: Discretization of a curve

7.2 System of Equations of Motion

We derive the system of ordinary differential equations which govern the motion of gliding dislocations.

Interior Points of the Curve

Integrating evolution equation (5.8) or (6.1) in dual volume $\mathcal{V}_i$ we get

$$\int_{\mathcal{V}_i} B\frac{\partial \mathbf{X}}{\partial t}\mathrm{d}s = \int_{\mathcal{V}_i} T\mathbf{X}_{ss}\mathrm{d}s + \int_{\mathcal{V}_i} F_{\text{eff}}\mathbf{X}^{\perp}\mathrm{d}s, \tag{7.1}$$

where we assumed a constant line tension T_i in dual volume $\mathcal{V}_i$. Then one obtains

$$B\frac{d_i + d_{i+1}}{2}\frac{\mathrm{d}\mathbf{X}_i}{\mathrm{d}t} = T_i\left[\mathbf{X}_s\right]_{\mathbf{X}_{i-\frac{1}{2}}}^{\mathbf{X}_{i+\frac{1}{2}}} + F_i\left[\mathbf{X}^{\perp}\right]_{\mathbf{X}_{i-\frac{1}{2}}}^{\mathbf{X}_{i+\frac{1}{2}}}. \tag{7.2}$$

$d_i = |\mathbf{X}_i - \mathbf{X}_{i-1}|$ is distance of the two neighbouring points $\mathbf{X}_i$ and $\mathbf{X}_{i-1}$ of the curve. F_i is a constant approximation of F_{eff} in dual volume $\mathcal{V}_i$ in corresponding point $\mathbf{X}_i$. Note, that F_i is the force per unit length of dislocation line. Now, we replace the term on the right-hand side by finite differences. Using the Taylor formulae

$$\mathbf{X}_i = \mathbf{X}_{i+\frac{1}{2}} - \frac{1}{2}d_{i+1}\left(\mathbf{X}_{i+\frac{1}{2}}\right)_s + O(d_{i+1}), \tag{7.3}$$

$$\mathbf{X}_{i+1} = \mathbf{X}_{i+\frac{1}{2}} + \frac{1}{2}d_{i+1}\left(\mathbf{X}_{i+\frac{1}{2}}\right)_s + O(d_{i+1}), \tag{7.4}$$

i.e. $\left(\mathbf{X}_{i+1/2}\right)_s = \left(\mathbf{X}_{i+1} - \mathbf{X}_i\right)/d_{i+1}$, $i = 1, \ldots, M-1$. $(\mathbf{X})_s$ means the derivative of $\mathbf{X}$ with respect to arc length parameterization s. Equation (7.1) can

be written in the form (using the definition of the points $\mathbf{X}_{i+1/2}$)

$$\begin{aligned} B\frac{\mathrm{d}\mathbf{X}_i}{\mathrm{d}t} &= \frac{2T_i}{d_i+d_{i+1}}\left(\frac{\mathbf{X}_{i+1}-\mathbf{X}_i}{d_{i+1}}-\frac{\mathbf{X}_i-\mathbf{X}_{i-1}}{d_i}\right)+\frac{2F_i}{d_i+d_{i+1}}\frac{\mathbf{X}_{i+1}^{\perp}-\mathbf{X}_{i-1}^{\perp}}{2}, \\ i &= 1,\ldots,M-1. \end{aligned} \tag{7.5}$$

We determine the line tension T_i from Eq. (4.7). Cosinus of α_i is determinate by the scalar product of the unit tangent to the curve at the point $\mathbf{X}_i$ and the unit vector in the direction of the Burgers vector:

$$\cos\alpha_i = (\mathbf{X}_i)_s \cdot \frac{\mathbf{b}}{b} \approx \frac{\mathbf{X}_{i+1}-\mathbf{X}_{i-1}}{d_i+d_{i+1}} \cdot \frac{\mathbf{b}}{b}\ . \tag{7.6}$$

Then we have $T_i = E_{\mathrm{edge}}\,(1-2\nu+3\cos^2\alpha_i))$.

End Points of the Curve

We will write the differential equation which govern the motion of the points $\mathbf{X}_0$ and $\mathbf{X}_M$, respectively. For these points we construct degenerate dual volumes, $\mathcal{V}_0^+ = \left[\mathbf{X}_0, \mathbf{X}_{1/2}\right]$ for point $\mathbf{X}_0$ and $\mathcal{V}_M^- = \left[\mathbf{X}_{M-1+1/2}, \mathbf{X}_M\right]$ for point $\mathbf{X}_M$. Integrating evolution equation (5.8) in degenerate dual volumes $\mathcal{V}_0^+$ and $\mathcal{V}_M^-$, one gets

$$B\frac{d_0}{2}\frac{\mathrm{d}\mathbf{X}_0}{\mathrm{d}t} = T_0\left[\mathbf{X}_s\right]_{\mathbf{X}_0}^{\mathbf{X}_{\frac{1}{2}}} + F_0\left[\mathbf{X}^{\perp}\right]_{\mathbf{X}_0}^{\mathbf{X}_{\frac{1}{2}}}, \tag{7.7}$$

$$B\frac{d_M}{2}\frac{\mathrm{d}\mathbf{X}_M}{\mathrm{d}t} = T_M\left[\mathbf{X}_s\right]_{\mathbf{X}_{M-1+\frac{1}{2}}}^{\mathbf{X}_M} + F_M\left[\mathbf{X}^{\perp}\right]_{\mathbf{X}_{M-1+\frac{1}{2}}}^{\mathbf{X}_M}. \tag{7.8}$$

To compute the terms $(\mathbf{X}_j)_s$, $j = 0, M$, we use the Taylor formulae

$$\mathbf{X}_1 = \mathbf{X}_0 + d_1\,(\mathbf{X}_0)_s + O(d_1), \tag{7.9}$$

$$\mathbf{X}_{M-1} = \mathbf{X}_M - d_M\,(\mathbf{X}_M)_s + O(d_M), \tag{7.10}$$

i.e. $(\mathbf{X}_0)_s = (\mathbf{X}_1-\mathbf{X}_0)/d_1$ and $(\mathbf{X}_M)_s = (\mathbf{X}_M-\mathbf{X}_{M-1})/d_M$. Note, that $(\mathbf{X}_0)_s = \left(\mathbf{X}_{1/2}\right)_s$ and $(\mathbf{X}_M)_s = \left(\mathbf{X}_{M-1+1/2}\right)_s$. These relations follow from Eqs. (7.3), (7.4), (7.9) and (7.10). So the first terms on the right-hand side of the Eqs. (7.7) and (7.8) vanish which is in agreement with the fact that for the straight segments $\left[\mathbf{X}_0, \mathbf{X}_{1/2}\right]$ and $\left[\mathbf{X}_{M-1+1/2}, \mathbf{X}_M\right]$ the curvature κ vanishes.

Now, if we use the definition of the points $\mathbf{X}_{j+1/2}$, $j = 0, M-1$, we can write the Eqs. (7.7) and (7.8) in the form

$$B\frac{\mathrm{d}\mathbf{X}_0}{\mathrm{d}t} = \frac{2F_0}{d_1+d_1}\left(\mathbf{X}_1^{\perp}-\mathbf{X}_0^{\perp}\right), \tag{7.11}$$

$$B\frac{\mathrm{d}\mathbf{X}_M}{\mathrm{d}t} = \frac{2F_M}{d_M+d_M}\left(\mathbf{X}_M^{\perp}-\mathbf{X}_{M-1}^{\perp}\right), \tag{7.12}$$

The evolution equations (7.5), (7.11) and (7.12) can be employed to govern the motion of discretized curve Γ_1. Similar equations hold also for curve Γ_2, if we replace $\mathbf{X}$ by $\mathbf{Y}$, line tension T by $\tilde{T}$ and the magnitude of effective force F_{eff} by $\tilde{F}_{\text{eff}}$.

Interaction Between Curves

We describe interaction term τ_{disl} by dislocation Γ_2 which act at a point $\mathbf{X}_i \in \Gamma_1$. $(F_i)_{\text{disl}}$ is a constant approximation of F_{disl} in dual volume $\mathcal{V}_i$, $i = 0, \ldots, M$:

$$\begin{aligned}(F_i)_{\text{disl}} &= b \int_{\Gamma_2} \mathrm{d}\tau_{\text{disl}} \approx b \sum_{j=0}^{M-1} \tau_{\text{disl}}^{[\mathbf{Y}_j \mathbf{Y}_{j+1}]} \\ &= b \sum_{j=0}^{M-1} \left(\tau_{\text{disl}} \left(\mathbf{R}_{\mathbf{Y}_j} \right) - \tau_{\text{disl}} \left(\mathbf{R}_{\mathbf{Y}_{j+1}} \right) \right). \end{aligned} \tag{7.13}$$

The last equality is consequence of Eq. (2.10). We marked $\mathbf{R}_{\mathbf{Y}_j}$ positional vector $\mathbf{R} = \mathbf{X}_i - \mathbf{Y}_j$. Remind that dislocation Γ_2 is oriented in the direction from point $\mathbf{Y}_M$ to $\mathbf{Y}_0$ whereas dislocation Γ_1 from point $\mathbf{X}_0$ to $\mathbf{X}_M$. The formula (7.13) for the force produced by another glide dislocation will be needed in the numerical simulation of the dislocation dynamics.

7.3 Applied Stress

As we mentioned in Section 4.5 we consider two limit cases. Either we control applied stress in the slip planes or we control the total shear strain. In the latter case, the applied stress resolved in the slip planes is given by relation (4.16) and during numerical simulations it is a unknown, which we have to determine. For this reason let us explain how we determine the applied stress during the computations when the total strain is controlled.

We assume a curve $\Gamma_1(t)$ at time t. Each discrete solution is represented by a moving polygon, it is a set of points $\Gamma_1(t) = (\mathbf{X}_0(t), \mathbf{X}_1(t), \ldots, \mathbf{X}_M(t))$. $M \in \mathbb{N}$ is fix. We want to compute a position of a curve at time $t + \tau$, i.e. $\Gamma_1(t + \tau)$. $\tau \equiv \Delta t$ is a constant time step and $\tau << t$. Denote $\Delta S_i(t)$ the approximation of an area slipped by a unit straight segment going through[1] the point $\mathbf{X}_i$ in time interval $(t - \tau, t)$. $S_i(t)$ is the approximation of the total area slipped by unit straight segment during evolution from $t_0 = 0$ to the

[1] $\mathbf{X}_i$ is a midpoint of segment

current position at time t, i.e. $S_i(t)$ is an area slipped after, say $N = t/\Delta t$ time steps: $S_i(t) = \sum_{k=1}^{N} \Delta S_i(k\tau)$. Let be a total shear strain a linear function of time, Eq. (4.17). The applied stress $(\tau_i(t+\tau))_{\text{app}}$ per unit length of dislocation line in dual volume $\mathcal{V}_i$ at time $t+\tau$ takes the form

$$(\tau_i(t+\tau))_{\text{app}} = \mu\varepsilon(t+\tau) - \mu\varrho b S_i(t). \tag{7.14}$$

By applying the rest of contributions[2] to the total stress acting on the dislocation at point $\mathbf{X}_i$, putting it to Eqs. (7.5), (7.11) and (7.12), we obtain using a solver a new solution $\Gamma_1(t+\tau)$ and whole procedure can be repeated. The contribution $\Delta S_i(t+\tau)$ we get in the following manner, see Fig. (7.2):

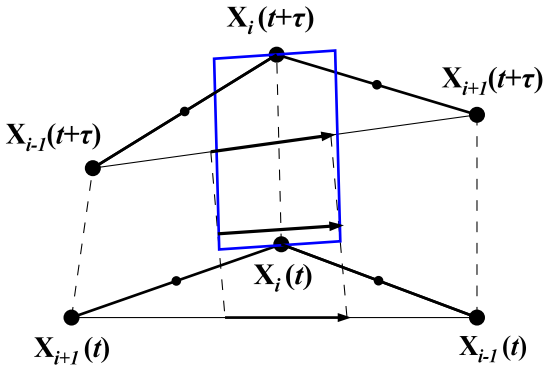

Figure 7.2: Slip area by an unit dislocation element in dual volume $\mathcal{V}_i$.

Area of a blue parallelogram is $\Delta S_i(t+\tau) = |\mathbf{n}_i \times \mathbf{s}_i|$, where we defined

$$\begin{aligned} \mathbf{n}_i &= \mathbf{X}_i(t+\tau) - \mathbf{X}_i(t), & (7.15)\\ \mathbf{s}_i &= \frac{1}{2}\left(\frac{\mathbf{X}_{i+1}(t+\tau) - \mathbf{X}_{i-1}(t+\tau)}{d_{i+1}(t+\tau) + d_i(t+\tau)} + \frac{\mathbf{X}_{i+1}(t) - \mathbf{X}_{i-1}(t)}{d_{i+1}(t) + d_i(t)}\right), & (7.16)\\ \text{for} \quad i &= 1, \ldots, M-1. \end{aligned}$$

and

$$\begin{aligned} \mathbf{n}_i &= \mathbf{X}_i(t+\tau) - \mathbf{X}_i(t), & (7.17)\\ \mathbf{s}_i &= \frac{1}{2}\left(\frac{\mathbf{X}_i(t+\tau) - \mathbf{X}_{i-1}(t+\tau)}{d_i(t+\tau)} + \frac{\mathbf{X}_i(t) - \mathbf{X}_{i-1}(t)}{d_i(t)}\right), & (7.18)\\ \text{for} \quad i &= 0, M. \end{aligned}$$

[2] $\tau_{\text{eff}} = \tau_{\text{app}} + \tau_{\text{disl}} + \tau_{\text{wall}}$

The symbol '$\times$' stands for the cross product of vectors, $|\mathbf{v}|$ is an Euclidean norm of the vector $\mathbf{v}$ and $d_i(t) = |\mathbf{X}_i(t) - \mathbf{X}_{i-1}(t)|$ is distance of the two neighbouring points $\mathbf{X}_i(t)$ and $\mathbf{X}_{i-1}(t)$ of the curve at time t.

7.4 Boundary and Initial Conditions

When not specify otherwise, initially both dislocation curves are kept apart in straight screw position. The initial configurations are naturally parameterized by the distance s and discretized:. Curve Γ_1 gliding in the 1$^{\text{st}}$ glide plane:

$$\begin{aligned} X_i^x(0) &= X^x(i\Delta s, 0) = i\Delta s + K^x, \\ X_i^y(0) &= X^y(i\Delta s, 0) = 0, \\ X_i^z(0) &= X^z(i\Delta s, 0) = K^z. \end{aligned} \tag{7.19}$$

and the curve Γ_2 gliding in the 2$^{\text{nd}}$ glide plane:

$$\begin{aligned} Y_i^x(0) &= Y^x(i\Delta s, 0) = i\Delta s + K^x, \\ Y_i^y(0) &= Y^y(i\Delta s, 0) = h, \\ Y_i^z(0) &= Y^z(i\Delta s, 0) = \tilde{K}^z. \end{aligned} \tag{7.20}$$

K^x, K^z and $\tilde{K}^z$, respectively, are real constants, h is spacing of glide planes and i goes from 0 to M. At the initial configuration the step length Δs is a constant and satisfy $M\Delta s = L(0)$. The position of each dipole was discussed in Section 3.2, Dislocation Walls.

The boundary conditions are select in a such a way that

$$\begin{aligned} X_i^x(t),\ i = 0, M \qquad & \text{no condition,} \\ X_i^y(t) = 0,\ i = 0, M \qquad & \text{for any time,} \\ \frac{\mathrm{d}X_i^z(t)}{\mathrm{d}t} = 0,\ i = 0, M \qquad & \text{for any time} \end{aligned} \tag{7.21}$$

for the curve $\Gamma_1(t)$ and

$$\begin{aligned} Y_i^x(t),\ i = 0, M \qquad & \text{no condition,} \\ Y_i^y(t) = h,\ i = 0, M \qquad & \text{for any time,} \\ \frac{\mathrm{d}Y_i^z(t)}{\mathrm{d}t} = 0,\ i = 0, M \qquad & \text{for any time} \end{aligned} \tag{7.22}$$

for the curve $\Gamma_2(t)$.

7.5 Solver

Eqs. (7.5), (7.11) and (7.12) can be formulate also in the form

$$\begin{aligned} \frac{\mathrm{d}\mathbf{X}_i}{\mathrm{d}t} &= f_i\left(t, F_{\mathrm{own}}(\Gamma_1, t), F_{\mathrm{eff}}(\Gamma_2, t)\right) \\ i &= 0, \ldots, M \end{aligned} \tag{7.23}$$

for the curve Γ_1 and

$$\begin{aligned} \frac{\mathrm{d}\mathbf{Y}_j}{\mathrm{d}t} &= \tilde{f}_j\left(t, \tilde{F}_{\mathrm{own}}(\Gamma_2, t), \tilde{F}_{\mathrm{eff}}(\Gamma_1, t)\right) \\ j &= 0, \ldots, M \end{aligned} \tag{7.24}$$

for the curve Γ_2. We labeled f_i and $\tilde{f}_j$ the right sides of equations of motion in corresponding points, where we write the implicit dependence on the current position of dislocations Γ_1 and Γ_2, respectively. To complete discrete problem consists of Eqs. (7.23) and (7.24) with accompanying initial and boundary conditions.

To solve this system of equations we employ the Runge-Kutta method of the 4^{th} degree. 4^{th} order Runge-Kutta formula was used in the form

$$\begin{aligned} k_1 &= g(t, u), \\ k_2 &= g\left(t + \frac{1}{2}\tau, u + \frac{1}{2}\tau k_1\right), \\ k_3 &= g\left(t + \frac{3}{4}\tau, u + \frac{3}{4}\tau k_2\right), \\ k_4 &= g(t + \tau, u + \tau k_3), \\ u(t + \tau) &= u(t) + \tau\frac{1}{6}(k_1 + 2k_2 + 2k_3 + k_4). \end{aligned} \tag{7.25}$$

Here, function $g \in \{f, \tilde{f}\}$ and u is a scalar function we want to evaluate.

Chapter 8

Results

We made several numerical simulations in which we use different settings. For the basic physical parameters we used values which were experimentally measured. They correspond to the structure of the PSB channel in copper crystal at a room temperature. The computations were performed with the following input data [**4, 23, 24**]:

– magnitude of the Burgers vector $b = 0.25$ nm,

– shear modulus $\mu = 42.1$ GPa,

– Poisson ratio $\nu = 0.43$,

– density of glide dislocations $\varrho = 9.2 \cdot 10^{12}$ m^{-2},

– energy of edge dislocation[1] $E_{\text{edge}} = 2.35 \cdot 10^{-9}$ Jm^{-1},

– drag coefficient[2] $B = 1.0 \times 10^{-5}$ Pa·s.

Notes to Analyse of Data

First of all we have to noticed that 'Effective stress' or 'Effective force' has different meaning than in Eq. (4.1). Let us denote effective force labeled by star as a sum of bowing and passing stress, that is

$$\tau^*_{\text{eff}} = \tau_{\text{bow}} + \tau_{\text{disl}}. \tag{8.1}$$

A discrete solution is a set of points which approximate the exact solution of the problem (4.1) with suitable boundary and initial conditions for each

[1] Using relation (1.3) for values b, μ, ν and $d_w = 0.15$ μm, Mughrabi [**4**]

[2] When not specified otherwise.

curve. Now, here is a question how to interpret the computation of effective stress τ^*_{eff} acting on each dislocation curve. It offers two possible points of view. We can either determine effective stress for one selected point on the curve, as in the model proposed by Mughrabi and Pschenitzka, or we can determine the average effective stress acting on the dislocation, as in the model proposed by Brown.

In each of these two approaches there are several questions:

In the first case one may ask which point has to be selected and if a information about the stress at this point gives adequate representation about resolved shear stress in the channel.

In the later approach there is following difficulty: Let us determine the average effective stress $\langle\tau^*_{\text{eff}}(t)\rangle$ as a function of slipped area by gliding dislocation. We consider the case when the stress is controlled and $\tau_{\text{app}} = \text{const}$. From Eq. (4.1) we have

$$Bv(t) = b\tau_{\text{app}} + b\tau^*_{\text{eff}}(t). \tag{8.2}$$

Integration of Eq. (8.2) along the curve gives

$$B\int v(t)\mathrm{d}s = b\tau_{\text{app}}\int \mathrm{d}s + b\int \tau^*_{\text{eff}}(t)\mathrm{d}s, \tag{8.3}$$

where $\int \mathrm{d}s = L(t)$ is the total length of the curve. B is a drag coefficient, b is the magnitude of Burgers vector. The average effective stress is

$$\langle\tau^*_{\text{eff}}(t)\rangle \equiv \frac{\int \tau^*_{\text{eff}}(t)\mathrm{d}s}{L(t)} = \frac{B}{bL(t)}\int v(t)\mathrm{d}s - \tau_{\text{app}}. \tag{8.4}$$

For the rate of change of slipped area by gliding dislocation holds relation

$$\frac{\mathrm{d}S(t)}{\mathrm{d}t} = \int v(t)\mathrm{d}s. \tag{8.5}$$

Now, let us imagine a situation that $\mathrm{d}S(t)/\mathrm{d}t = \text{const}$. Then from Eq. (8.4) follows that $\langle\tau^*_{\text{eff}}(t)\rangle = -\tau_{\text{app}}$, since during evolution of curve $L(t) \to \infty$ as $t \to \infty$, which is impossible. The problem results from the method of computation of the length of the curve. We counted to $L(t)$ parts of dislocation which does not contribute to slip area. To solve this problem it is suitable to count just the length of leading curved part $\beta\gamma$ of dislocation, see Fig. 1.1. But this approach is not suitable for our problem, since it is difficult to check which points $\mathbf{X}_i$ are on the leading curved part of dislocation.

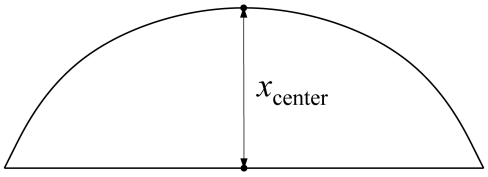

Figure 8.1: The arrow shows the trajectory of the midpoint of the dislocation.

For the reasons mentioned above we chose the first approach proposed by Mughrabi and Pschenitzka. We represent the results for the point in the middle of the first curve Γ_1. Because of symmetry of the geometry the same results may be obtained if one choose the middle of the second dislocation. The choice of this point has several reasons: (1) At the centre of the curve we have a good information about instantaneous velocity of the dislocation; (2) the interaction stress between the two curved dislocations experience the maximum at the centre of the channel; (3) the stresses from the walls vanishes, in contrast to another point on the curve which drift to the wall on the right-hand side or left-hand side, Fig. 3.1.

The results will be discussed with respect to the trajectory x_{centre} of the point in centre of the dislocation Γ_1, see Fig. (8.1)

8.1 Numerical Simulations

8.1.1 Simulations at Constant Spacing Between Slip Planes

Simulation 1

In this section we present results we got for the parameters, Eqs. (7.19) and (7.20), (all distances are measured in nanometers): $K^x = -480$, $K^z = 0$, $\tilde{K}^z = -1000$. Starting with a straight dislocation lines. The length step $\Delta s = 4$ and $i = 0, \ldots, 241$. We approximated each curve by 240 points, initially equidistantly distributed on the curve. The initially length $S(0)$ of each curve was 960 nm. The midpoints of the dipoles were set up to the distance 25 nm from corresponding end points of the curves. The spacing between slip planes $h = h_c = 55$ nm, walls spacing $d_c = 960$ nm.

Observation 1.1

Let us consider the case when we control the applied stress and

$$\tau_{\text{app}} = \text{const.}$$

If the external stress is small comparing to the line tension of the dislocation curve, the motion stops after a certain time. It stops in a position where the external stress and the effective stress τ^*_{eff} are in an equilibrium state.

When the external (applied) stress is switched off, the curvature pushes the dislocation curve back to its initial position, i.e. straight line.

First observation is, that the motion depends on dimensions of the dislocation curves and the size of external stress.

Observation 1.2

As positions of the curve end points are restricted by boundary conditions, Eqs. (7.21) and (7.22), initial straight line becomes curved as the time flows. We observe curvature of the curve (elastic stress of the dislocation) to partly eliminate the external stress, so the curves are not moving with the same speed everywhere. The bigger the curvature is, the slower is the response to the external stress.

Observation 1.3

We assume a constant external stress $\tau_{\text{app}} = 40$ MPa was applied for the whole time of computation. Fig. 8.2 shows the two dimensional plot of evolution of curves from initial straight configurations. The pairs of double black lines representing the positions of dislocation dipoles.

In Fig. 8.2 - b. we can observe strong change of the shapes of the dislocations due to interaction between curves. When the dislocations are close to enough, they attract one another and if their curvature is not great (it depends also on the width of the channel) they can forming a dipole, see Fig. 8.2 - b.

Observation 1.4

Again, we assume a constant external stress, $\tau_{\text{app}} = 40$ MPa. The most significant for the shapes of the curves is their relative position to each other.

Both dislocation curves produce a stress field which interact with the second one. We consider the two situations: the case when we consider

interaction between curves and the second case when we neglected this contribution to the effective stress. Fig. 8.3 compares the shapes of the curves in these two cases. Fig. 8.3 - a. shows the shapes of the dislocation curve Γ_1 when we consider interaction between curves, while Fig. 8.3 - b. shows the situation when the interaction term is neglected.

The observation is, that there is a distance threshold behind which there is almost no interaction between curves and they do not interact as they are far enough from each other.

Observation 1.5

Now, assume two simulations, depending on the external stress: in the first case we assume the applied stress is controlled, $\tau_{\text{app}} = 40$ MPa; in the second case we assume the total shear strain is controlled, $\mathrm{d}\varepsilon_{\text{tot}}/\mathrm{d}t = 2.85 \cdot 10^{-3}$.

Fig. 8.4 - a. compares the shapes of the curves in these two limit cases. The red lines correspond to the first case, the blue one to the second case. Well, it is not to easy doing some conclusions when the shapes of curves depend on the size of applied stress.

Observation 1.6

Two measurements of effective stress $\tau^*_{\text{eff}}(x_{\text{center}})$ have been done. In the first case the applied stress was controlled, $\tau_{\text{app}} = 44$ MPa; in the second case the total shear strain was controlled, $\mathrm{d}\varepsilon_{\text{tot}}/\mathrm{d}t = 2.85 \cdot 10^{-3}$.

Fig. 8.5 - a. shows the results. We plot the effective stress as a function of a trajectory of the midpoint of the curve Γ_1 in the 1^{st} glide plane. The effective stress resulting from superposition of the bowing stress $\tau_{\text{bow}}(x_{\text{center}})$ and the dipolar interaction stress $\tau_{\text{dip}}(x_{\text{center}})$.

At $x_{\text{center}} = 500$ nm is a meeting point of the middle points of the curves. In Fig. 8.5 - a. we can see that for $x_{\text{center}} \in (0, 300\text{ nm})$ dominate the curvature term τ_{bow}, while for $x_{\text{center}} \in (300\text{ nm}, 700\text{ nm})$ dominate the dipolar term τ_{dip}. The effective stress is a sum of these contributions, Eq. (8.1).

The maximum of the effective stress in the first case is about 33 MPa, in the second case about 28.7 MPa. These two maxima gives the upper and lower stress bound of the endurance limit.

Observation 1.7

We assume similar conditions as in Observation 1.6, i.e, in the first series of simulations $\tau_{\text{app}} = 44$ MPa; in the second series of simulations $\mathrm{d}\varepsilon_{\text{tot}}/\mathrm{d}t = 2.85 \cdot 10^{-3}$.

In both cases we assume that the interaction term between the curves can be neglected, i.e. $\tau_{\text{dip}} = 0$. Then the effective stress τ^*_{eff} is equal to the bowing stress τ_{bow}.

Fig. 8.5 - b. shows a bowing stress as a function of x_{center}. Notice that the results are in agreement with the shapes of the curves in Fig. 8.4 - a.

Observation 1.8

Finally of Simulation 1, consider four different settings: (1) the applied stress is controlled, $\tau_{\text{app}} = 40$ MPa; (2) the applied stress is controlled, $\tau_{\text{app}} = 40$ MPa and we neglected the interaction between curves; (3) the total shear strain is controlled, $\mathrm{d}\varepsilon_{\text{tot}}/\mathrm{d}t = 2.85 \cdot 10^{-3}$; (4) the total shear strain is controlled, $\mathrm{d}\varepsilon_{\text{tot}}/\mathrm{d}t = 2.85 \cdot 10^{-3}$ and we neglected the interaction between curves.

Comparison of velocity of the centre of the curve Γ_1 in all four cases gives Fig. 8.4 - b.

From Fig. 8.4 - b. we can easy determine when the dislocation strongly attract one another.

Simulation 2

In two series of measurements we explore different values of the width spacing d_c at constant spacing between the slip planes. This part is maybe the most interesting one. We can see that in decreasing the channel spacing, the critical (maximum) effective stress is increased.

Observation 2.1

In the first experiment, following setting of parameters (units in nm) were used: $K^x = -330$, $K^z = 0$, $\tilde{K}^z = -1000$. Starting with straight dislocation lines, initially length of each curve is 660 nm.

When the applied stress is controlled, each curve is approximate by 221 points, initially equidistantly distributed with nodes $\Delta s = 3$ nm. $\tau_{\text{app}} = 60$ MPa.

When the total shear stress is controlled, each curve is approximate by 221 points, initially equidistantly distributed with nodes $\Delta s = 3$ nm. $\mathrm{d}\varepsilon_{\text{tot}}/\mathrm{d}t = 2.85 \cdot 10^{-3}$.

Fig. 8.6 - a. shows the results. In the first case the maximum of the effective stress is about 46.4 MPa, in the later case 44.4 MPa.

Observation 2.2

The second experiment has been done for values of parameters (unit in nm): $K^x = -1000$, $K^z = 0$, $\tilde{K}^z = -1200$. Starting with a straight dislocation lines, initially length of each curve is 2000 nm.

When the applied stress is controlled, each curve is approximate by 201 points, initially equidistantly distributed with nodes $\Delta s = 10$ nm. $\tau_{\text{app}} = 32$ MPa.

When the total shear stress is controlled, each curve is approximate by 401 points, initially equidistantly distributed with nodes $\Delta s = 5$ nm. $\mathrm{d}\varepsilon_{\text{tot}}/\mathrm{d}t = 2.85 \cdot 10^{-3}$.

Fig. 8.7 - a. shows the results. In the first case the maximum of the effective stress is about 21.4 MPa, in the later case 17.5 MPa. Fig. 8.7 - b. compares the shapes of curves at $x_{\text{center}} = 1000$ nm in the two limit cases.

Observation 2.3

Figs. 8.5 - b., 8.6 - b. and 8.8 - b. show the bowing stress as a function of x_{center} with different values of width of channel, $d_c = 960$ nm, $d_c = 660$ nm and $d_c = 2000$ nm.

We can see, that the bowing stress increases as the width of channel is decreasing.

Simulation 3

One may ask how much the values of drag coefficient or strength of applied stress influence the effective stress. Fig. 8.9 gives satisfactory explanation.

Fig. 8.9 - a. shows results with different settings of drag coefficient ($B = 2 \cdot 10^{-5}; 10^{-5}; 5 \cdot 10^{-6}$ and 10^{-6} Pa·s) in case when the total shear strain was controlled. Note that in decreasing drag coefficient the velocity of dislocation curves increase.

Fig. 8.9 - b. shows results with different settings of applied stress (30; 34 and 40 MPa) and total shear strain ($\mathrm{d}\varepsilon_{\text{tot}}/\mathrm{d}t = 3 \cdot 10^{-3}; 6 \cdot 10^{-3}$ and $9 \cdot 10^{-3}$).

The observation of these simulations is that the effective stress does not depend strongly upon the values of the external parameters as drag coefficient, applied stress or total shear strain.

8.1.2 Simulations at Constant Width of PSB Channel

If we fix the channel spacing and consider glide planes closer and closer, the influence of the interaction stress is clearly dominant. At small value of spacing h between glide planes, the critical passing position is mainly fixed by the interaction stress between the two screw parts.

We consider an experiment where we controlled the applied stress, $\tau_{\text{app}} = 44$ MPa. Settings: as in Simulation 1.

Fig. 8.8 - b. shows the results with three different settings of h. The maxima of the effective stress are 33 MPa for $h = 55$ nm, 25 MPa for $h = 155$ nm and 18.9 MPa for $h \to \infty$. Notice that at x_{center} the graphs of effective stress interact each other since at x_{center} the point in the middle of curve experiences[3] just bowing stress.

8.1.3 Comparison results with Mughrabi

We made experiment with the same setting of parameters as in paper [**4**] by Mughrabi: shear modulus $\mu = 42$ GPa, the magnitude of Burgers vector $b = 0.25$ nm, constant line tension $T = 2.5 \cdot 10^{-9}$ N, spacing between the glide planes $h = 55$ nm, the width of channel $d_c = 950 - 960$ nm. Mughrabi consider the largest possible dipole interaction (maximum value of the dipole passing stress) $\tau_{\text{dip}} = 15$ MPa.

Fig. 8.9 - b. compares our results with Mughrabi's calculations. For our simulations we used different settings[4] of τ_{app} and ε_{tot}.

[3] Because of symmetry of geometry.

[4] $\tau_{\text{app}} = 30, 34$ and 40 MPa, $\mathrm{d}\varepsilon_{\text{tot}}/\mathrm{d}t = 0.003, 0.006$ and 0.009.

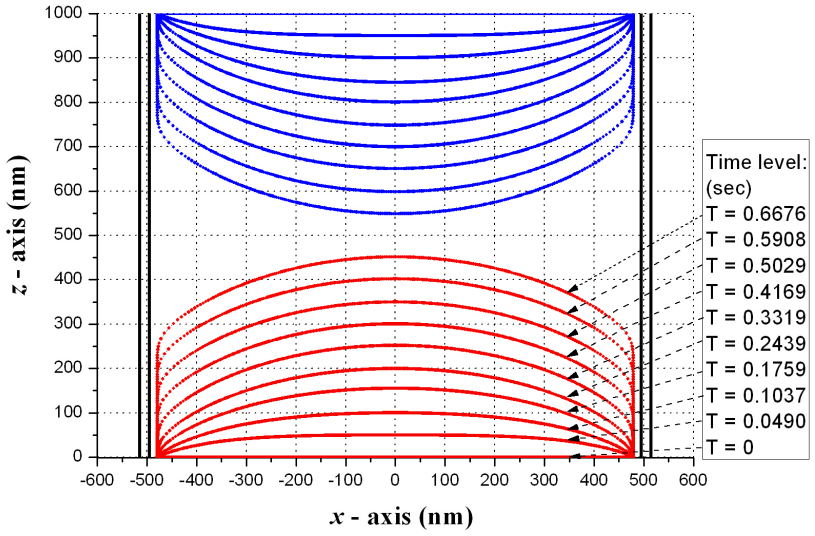

(a.)

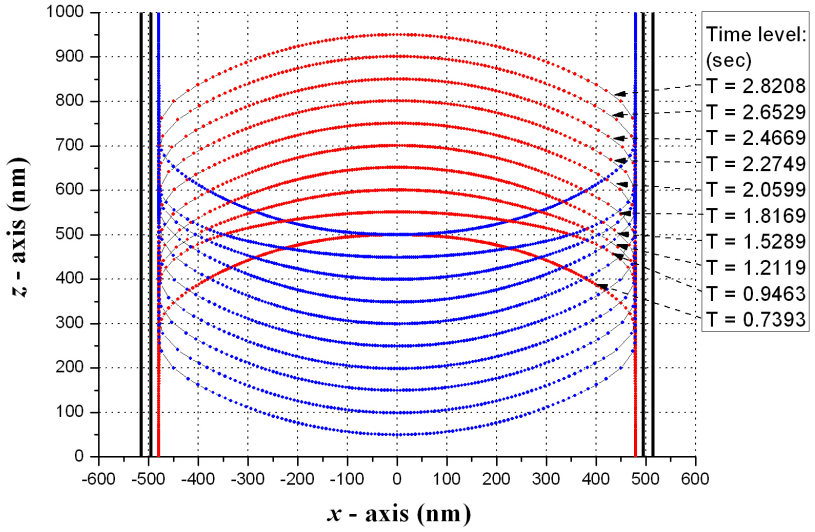

(b.)

Figure 8.2: The expanding dislocations in the case when the stress is controlled. The time intervals are (a.) $t \in (0, 0.7)$ and (b.) $t \in (0.7, 3)$.

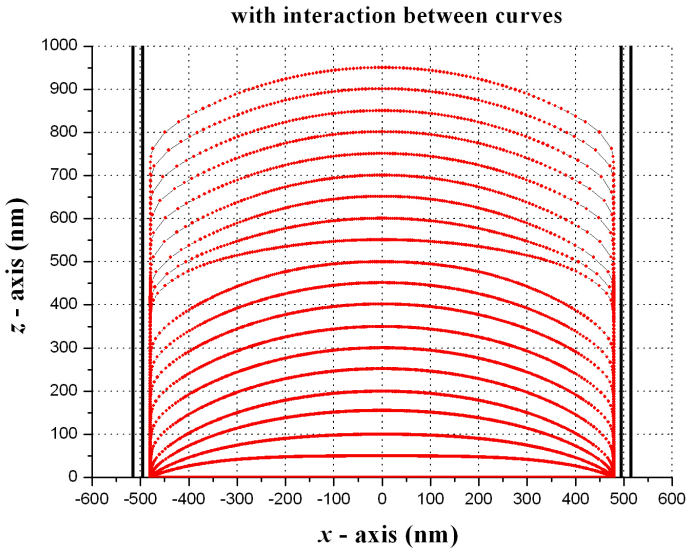

(a.)

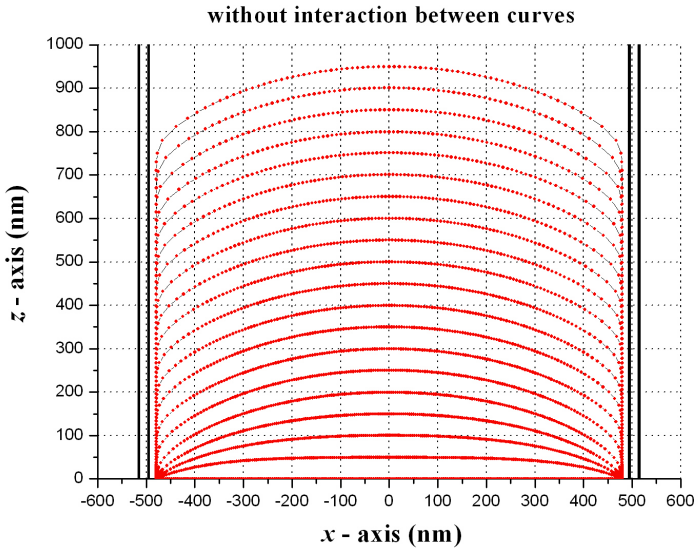

(b.)

Figure 8.3: Figures (a.) and (b.) compare the shapes of the curves. In both cases the stress was controlled, but in the later case we neglected the interaction between gliding dislocations.

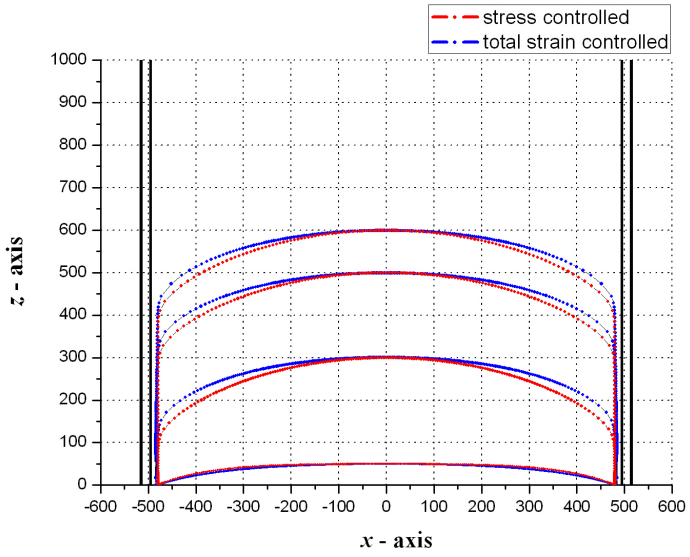

(a.)

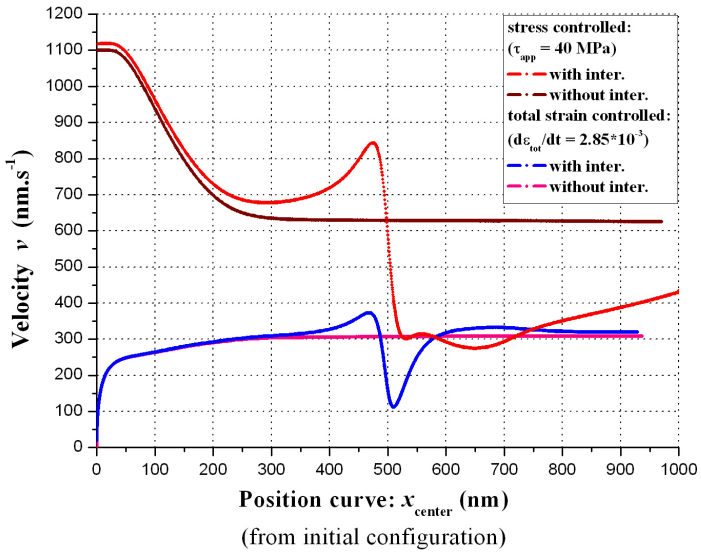

(b.)

Figure 8.4: (a.) Comparison of the shapes of a curve in the two limit cases (stress controlled - red lines, total shear strain controlled - blue lines) (b.) Comparison of the velocities as function of x_{center} in two cases: with and without interaction between gliding dislocations.

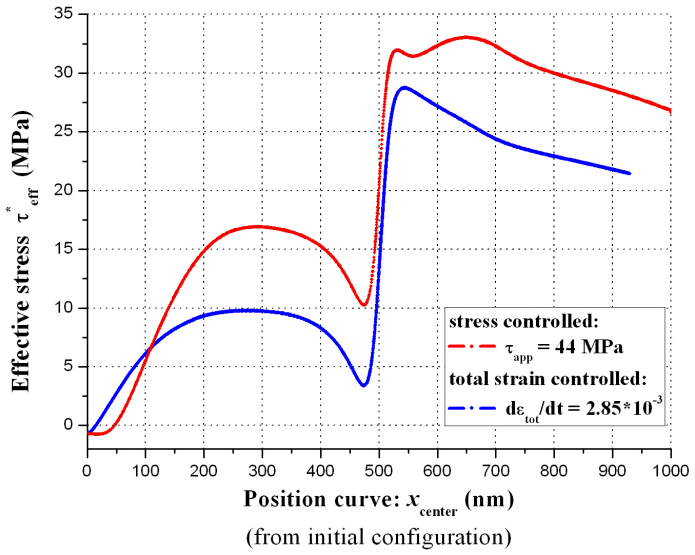

(a.)

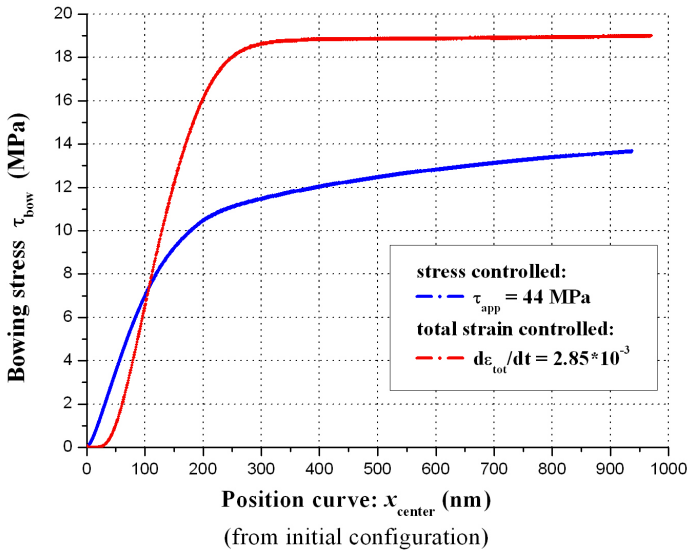

(b.)

Figure 8.5: (a.) The width of channel is 960 nm. Effective stress as a function of x_{center} in the two limit cases (the stress controlled - red line, the total shear strain controlled - blue line) (b.) We neglected the interaction between the gliding dislocation. It describes just bowing stress.

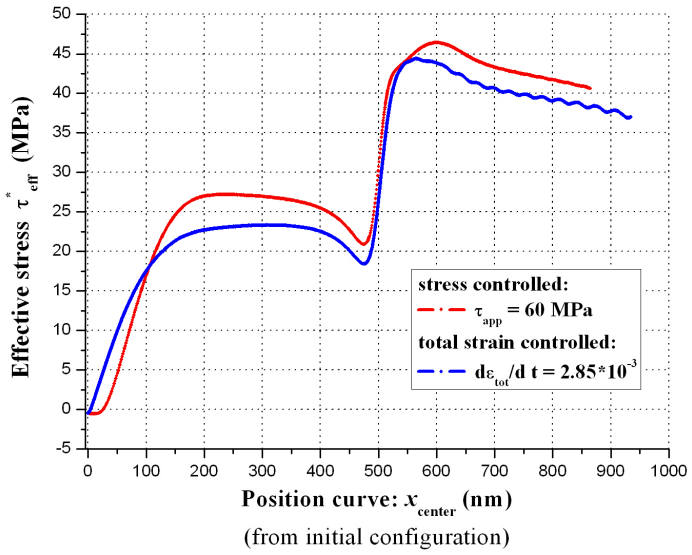

(a.)

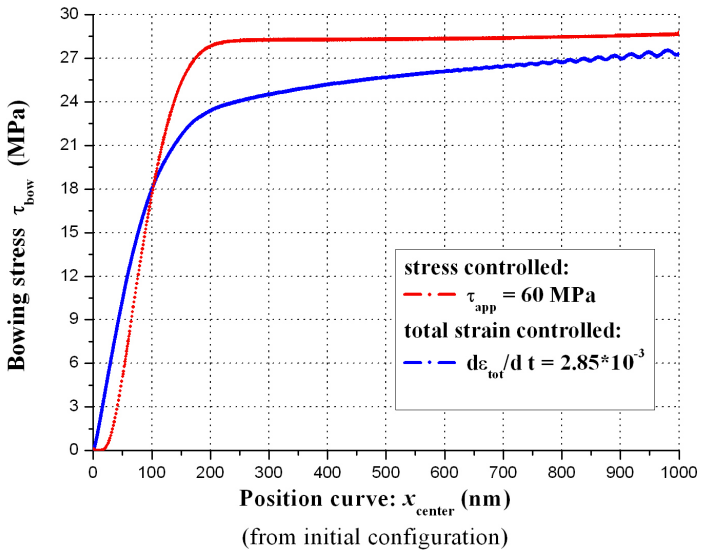

(b.)

Figure 8.6: (a.) The width of channel is 660 nm. Effective stress as a function of x_{center} in the two limit cases (the stress controlled - red line, the total shear strain controlled - blue line) (b.) We neglected the interaction between the gliding dislocations. It describes just bowing stress.

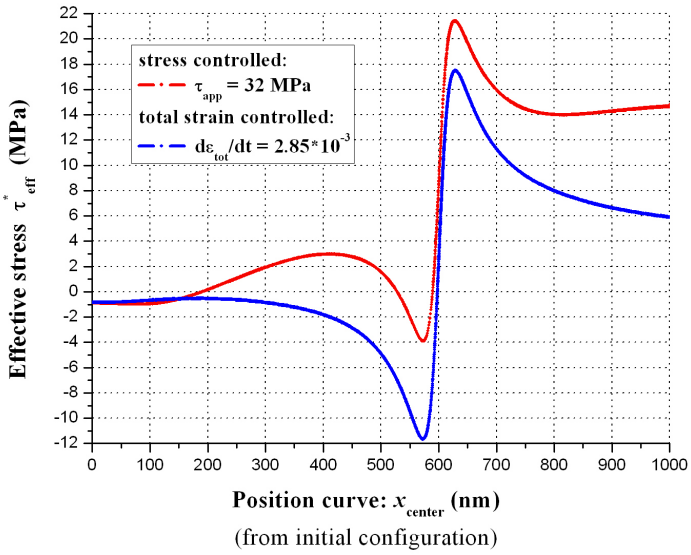

(a.)

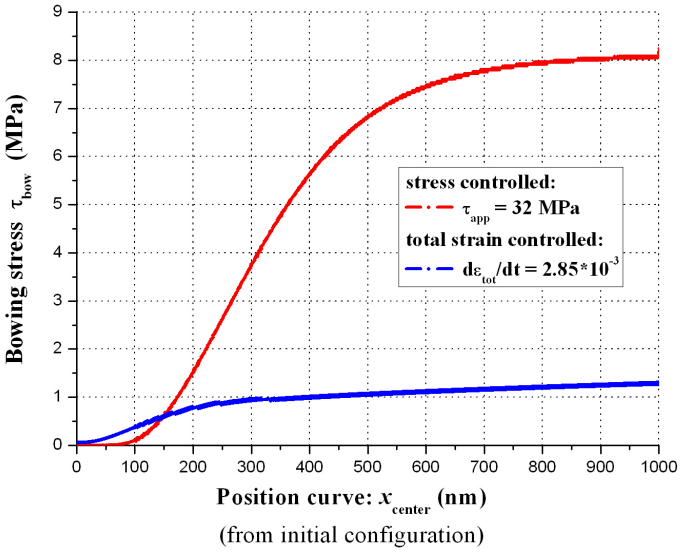

(b.)

Figure 8.7: (a.) Effective stress as a function of x_{center} in the two limit cases (the stress controlled - red line, the total shear strain controlled - blue line); the width of channel is 2000 nm. (b.) We neglected the interaction between the gliding dislocations. It describes just bowing stress.

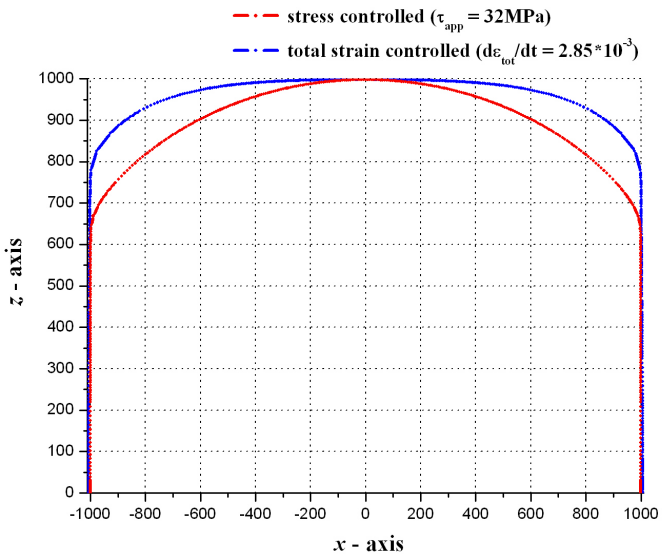

(a.)

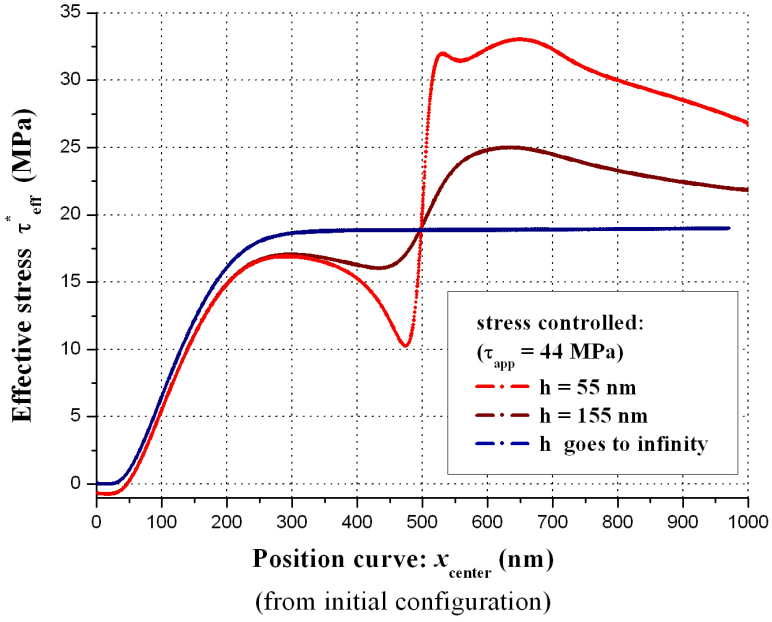

(b.)

Figure 8.8: (a.) Comparison of the shapes of curves in the two limit cases (stress controlled - red lines, total shear strain controlled - blue lines) with $d_c = 2000$ nm. (b.) Evolution of the effective stress in the glide plane as a function of spacing between glide planes at constant width of channel.

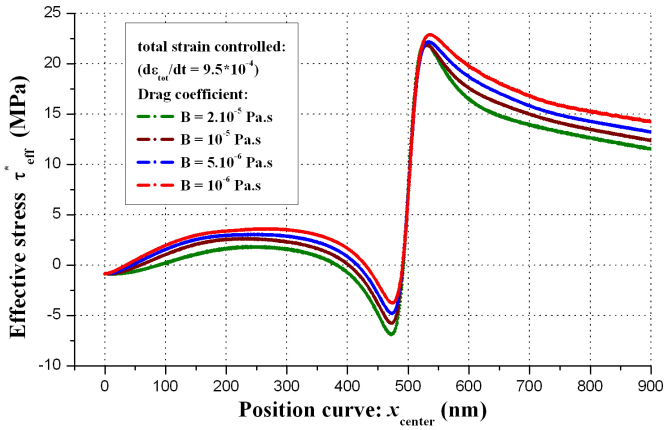

(a.)

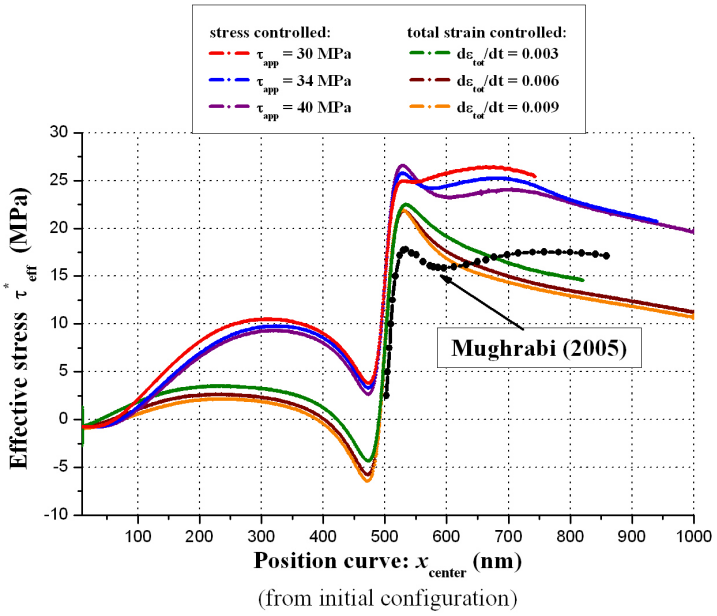

(b.)

Figure 8.9: (a.) Effect of variations of drag coefficient on the effective stress in case when the total shear strain is controlled. (b.) Comparison results with Mughrabi.

Chapter 9

Conclusions

The present work was motivated by the need to obtained some extended information about the motion of two dislocations of opposite sign in the PSB channel and to estimate the effective resolved shear stress in a slip plane. The proposed computer program provides the possibility to simulate the motion of interacting dislocations under the stress or total strain controlled conditions. For the standard concepts ('bowing' stress, 'dipolar passing' stress, 'local flow' stress in PSB channel) we got order of magnitude estimates, which are in a reasonable agreement with the results of Brown [**2**] and Mughrabi & Pschenitzka [**4**]. I hope, the present work extends previous studies, in particular the work by Brown [**2**] and Mughrabi & Pschenitzka [**4**].

The mathematical model has been derived for two limit conditions of the motion of gliding dislocations in the PSB channel: (i) the motion with the constant applied stress, (ii) the motion with the homogeneous total shear strain. An evolution equation for a curved glide dislocation is formulated using the concept of line tension and a parametric description of the dislocation line.

We suggested the model where we took into account the structure of the walls in the PSB channel. Next we suggested possible way how to compute the stress produced by gliding dislocation.

The equation of motion of a curved glide dislocation was developed into a form suitable for computation of the glide dislocation evolution.

Summary of Results and Discussion

The present dislocation dynamics simulations have allowed to us to study dislocation-dislocation interactions in ways not possible using analytical ap-

proaches. We find that the interactions are dominated by configuration changes which are sensible and straightforward to interpret in retrospect, but which would have been difficult to predict using simple analytical tools.

Computer time

The time complexity of numerical simulations is order of $O((N-1)^2)$, where N is the number of points on the each curve. The most costly procedure, in terms of computer time, consists of calculating the stress field of the segments, Eqs. (2.9), (2.10). In each time step we compute the stress from $2(N-1) \times (N-1)$ dislocation straight segments.

Main results

The main results of our study are:
(i) The effective stress does not depend strongly upon the values of the external parameters as drag coefficient, applied stress or total shear strain.
(ii) In decreasing the channel spacing at constant spacing between glide planes, the maximum of passing stress is increased.
(iii) At constant width of channel and consider glide planes closer and closer, the influence of the interaction stress is dominant.
(iv) Maximum values of the effective stress (in units MPa) which were determined are summarized in table:

h (nm)	d_c (nm)	stress controlled	strain controlled
55	660	46.4	44.4
55	960	33	28.7
55	2000	21.4	17.5
155	960	25	-
∞	660	28.3	27.5 and grow
∞	960	18.9	13.7 and grow
∞	2000	8.1	1.3 and grow

(v) Fig. 8.9 - b. gives estimate for the effective stress in real situation 21.5 MPa $< \tau_{\text{real}} <$ 26.6 MPa. Then from Eq. (1.26) derived by Brown one may gets[1] estimate of coefficient α: $0.65 < \alpha < 0.16$. Brown estimates $\alpha = 0.5$.
(vi) Boundary conditions also have a significant effect on the configurations adopted by dislocations.

[1]With suitable values of d_c, h, μ, b and E_{edge}.

Outlook

To analyze and construct a computer program of boundary controlled case, i.e. to combine the present program with FEM.

To replace the distance between the dislocation centers by the area swept by dislocations as a controlled variable.

To introduce moving dipolar dislocation loops in the PSB channel.

Bibliography

[1] Pant, P., Schwarz, K. W., Baker, S. P., Dislocation Interactions in Thin FCC Metal Films, *Acta Mater.* **51** (2003), 3243-3258

[2] Brown, L. M., Dislocation Bowing and Passing in Persistent Slip Bands, *In press*

[3] Brown, L. M., *Mater. Sci. Eng. A* **285** (2000), 35

[4] Mughrabi, H., Pschenitzka, F., Constrained Glide and Interaction of Bowed-Out Screw Dislocation in Confined Channels, *Special Issue of Philosophical Magazine* **85** (2005), 3029

[5] Mughrabi, H., Levine, L., Kubin, L., Becker, R., Dislocations 2000, *Mater. Sci. Eng.* **A 309 - 310** (2001), 237

[6] Peach, M., O., Koehler, J., S., *Phys. Rev.* **80** (1950), 436

[7] R. de Wit, *Acta Metall.* **13** (1965), 1210

[8] R. de Wit, Some Relations for Straight Dislocations, *Phys. Stat. Sol.* **20** (1967), 567-570

[9] Gage, M., Hamilton, R. S., The Heat Equation Shrinking Convex Plane Curves, *J. Diff. Geom.* **23** (1986), 69-96

[10] Verdier, M., Fivel, M., Groma, I., Mesoscopic Scale Simulation of Dislocation Dynamics in fcc Metals: Principles and Applications, *Modelling Simul. Mater. Sci. Eng.* **6** (1998), 755-770

[11] R. de Witt, G., Koehler, J. S., *Phys. Rev.* **116** (1959), 1113

[12] Sedláček, R., Viscous Glide of a Curved Dislocation, *Philosophical Magazine Letters* Vol. **76** No. **4** (1997), 275-280

[13] Alshit, V. I., Indesbom, V. L., Dislocations in Solids, Vol. **7** ed F. R. N. Nabarro (1979), Amsterdam

[14] Tippetl, B., Bretschneider, J., Hähner, P., The Dislocation Microstructure of Cyclically Deformed Nickel Single Crystal at Different Temperatures, *Phys. Stat. Sol. (a)* **163** (1997), 11-26

[15] Minárik, V., Kratochvíl, J., Mikula, K. and Beneš, M., Numerical Simulation of Dislocation Dynamics, *the* 5^{th} *European Conference on Numerical Mathematics and Advanced Applications* (2003), 631-640

[16] Deckelnick, K., Dziuk, G., Discrete Anisotropic Curvature Flow of Graphs, *Math. Modelling Numer. Anal.* **33** (1999), 1203-1222

[17] Sethian, J. A., Level Set Method and Fast Marching Methods, Downloaded from: http://math.berkeley.edu/šethian/level_set.html

[18] Dziuk, G., Schmidt, A., Brillard, A., Bandle, C., Course on Mean Curvature Flow, Freiburg, January 8 (1994)

[19] Verecký, Š., Kratochvíl, J., Kubin, L.P., The Sweeping of a Dipolar Loop by a Glide Dislocation in a PSB Channel, *Journal de Physique IV France* **11** (2001), 35-41

[20] Verecký, Š., Dislocation Mechanism of Cyclic Plasticity of Materials *Final Year Thesis* (2002), MFF UK

[21] Mikula, K., Ševčovič, D., Evolution of Plane Curves Driven by a Nonlinear Function of Curveture and Anizotropy, *SIAM J. Appl. Math.* Vol. **61** No. **5** (2001), 1473-1501

[22] Dziuk, G., Convergence of a Semi Discrete Scheme for the Curve Shortening Flow, *Mathematical Models and Methods in Applied Sciences* No. **4** (1994), 589-606

[23] Sansal, C., Devincre, B., Passing Stress of Bowed-out Screw Dislocations in Confined Channels, *Use for Vienna talk,* 17^{th} *Colloquium on Fundamental Fatigue Mechanisms 2006* (January, 2006)

[24] Scattergood, R.O. and Bacon, D.J, *Phil. Mag.*, **31** (1975), 179

[25] Kroupa, F. and Machová, A., Fyzika kovů I (Teorie dislokací), 38 (1988)

[26] Dekker, A.J., Fyzika pevných látek, kap. 1-3, *Academia* (1966)

[27] Verecký, Š., Kratochvíl, J., Kroupa, F., The Stress Field of Rectangular Prismatic Dislocation Loops, *Phys. Stat. Sol. (a)* **191** No. **2** (2002), 418-426

[28] Minárik, V., Kratochvíl, J. and Mikula, K., Numerical Simulation of Dislocation Dynamics by Means of Parametric Approach, *Proceedings of the Czech-Japanese Seminar in Applied Mathematics 2004*, 1-8 (2004)

[29] Huang, J., Ghoniem, N.M., Kratochvíl, J., On the Sweeping Mechanism of Dipolar Dislocation Loops Under Fatigue Conditions, *Modelling Simul. Mater. Sci. Eng.* **12** (2004), 1-12

[30] R. de Wit, The Self-Energy of Dislocation Configurations Made up of Straight Segments, *Phys. Stat. Sol.* **20** (1967), 576

[31] Brown, L. M., A Discusssion of the Structure and Behaviour of Dipole Walls in Cyclic Plasticity, *Philosophical Magazine* Vol. **84** No. **24** (2004), 2501-2520